A Viscoelastic Approach for the Characterization of Bending Behavior of Uncured Unidirectional Carbon/Epoxy Prepreg

Seyed Amirreza Pakzadi

A Thesis in

The Department

of

Mechanical, Industrial, and Aerospace Engineering

Presented in Partial Fulfillment of the Requirements

for the Degree of Master of Applied Science in Mechanical Engineering at

Concordia University

Montreal, Quebec, Canada

October 2021

© Seyed Amirreza Pakzadi, 2021

CONCORDIA UNIVERSITY

School of Graduate Studies

This is certify that the thesis prepared

By: Seyed Amirreza Pakzadi

Entitled: A Viscoelastic Approach for the Characterization of Bending Behavior of Uncured Unidirectional Carbon/Epoxy Prepreg

And submitted in partial fulfillment of the requirements for the degree of

Master of Applied Science (Mechanical Engineering)

Complies with the regulations of this University and meets the accepted standards with respect to originality and quality.

Signed by the final Examining committee:

Chair

Dr. Tsz Ho Kwok

Examiner

Dr. Tsz Ho Kwok

External Examiner

Dr. Anjan Bhowmick

Supervisor

Dr. Mehdi Hojjati

Approved by

Dr. Martin D. Pugh
Chair, Department of Mechanical, Industrial & Aerospace Engineering

October 5, 2021

Dr. Mourad Debbabi, Dean
Gina Cody School of Engineering and Computer Science

Abstract

A Viscoelastic Approach for the Characterization of Bending Behavior of Uncured Unidirectional Carbon/Epoxy Prepreg

Seyed Amirreza Pakzadi

High demands of composites application in various industries have led to top-quality manufacturing techniques, including automated fiber placement and double diaphragm forming. These advanced technologies are restrained by defects formation during the layup and forming process. Several studies have been conducted to investigate the effect of process parameters and to identify the different forming mechanisms for better understanding defect formation. Among these parameters, the bending property of uncured prepreg is the primary factor that can dominate the most common emerging defect known as wrinkle during composite forming. Perceiving these properties in depth could reduce the costs of the experiment extensively as they could be proper input for simulation software to have better defect prediction. Since composites are classified as viscoelastic materials, the main goal of this thesis is to study the effect of viscoelasticity on the bending stiffness of uncured carbon epoxy prepreg. For this purpose, a stress relaxation test has been implemented using a tensile test machine at room and elevated temperatures. Also, the effect of temperature on the viscoelastic behavior of the sample is discussed. In conformity with the experimental observations, a new nonlinear viscoelastic model is proposed and compared to linear models. It is shown that this proposed model is able to address viscoelastic behavior not only in the prior and after elastic region but also out of the testing time range. Within this thesis, a bending test method for defining the bending behavior of prepreg materials at forming conditions was developed based on a horizontal cantilever beam. Then, both linear and nonlinear aspects have been coupled with constitutive bending equations to represent the bending behavior and its time dependency. At last, a finite element (FEM) is performed in the ABAQUS platform in order to depict the results correlations. Moreover, a simple deformation mechanism has been simulated to represent the effect of deformation rate perfectly.

ACKNOWLEDGEMENTS

First of all, I would like to express my most profound appreciation to my supervisor Dr. Mehdi Hojjati for his exceptional support and guidance throughout this program. The present work would not be attainable without him.

I like to thank Dr. Daniel-Iosif Rosca and Dr. Heng Wang for their support in performing the experiments. Moreover, I would like to thank my friends and colleagues from Concordia Center for Composites, especially Mr. Mohammad Hossein Ghayour, for their collaboration and discussions on the topic.

Last but not least, my heartfelt thanks to my parents for their endless love, support, and continuous encouragement throughout this journey.

DEDICATION

To my beloved parents

TABLE OF CONTENTS

LIST OF FIGURES

LIST OF TABLES

1 Introduction

1.1 Background and motivation

These days, composite materials have been widely adopted as a primary material in designing and manufacturing load-bearing structures in several industries such as aerospace and automotive. Consequently, the significant advancement of aircraft design is owing to the application of composite. For instance, Figure 1.1 illustrates the rapidly increasing application of composite materials in military and civil aircraft [1].

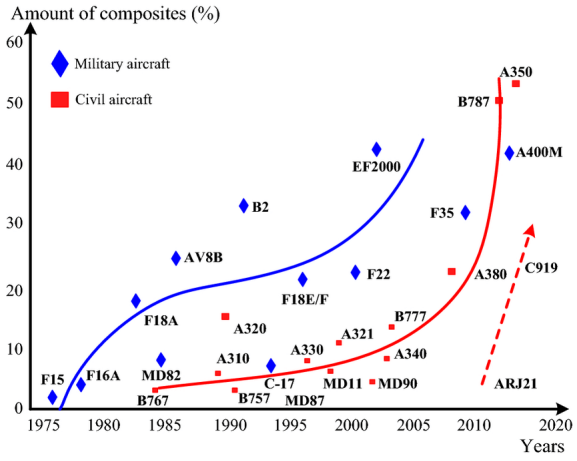

Figure 1. 1: Amount of composites material used in military and civil aircraft [1]

Moreover, the worldwide statistic indicates the market value of composite materials in 2015, 2017, and 2019, with a prediction for 2027 (Figure 1.2). It was forecasted that the global market size for composites would amount to 160.54 billion U.S. dollars in 2027 [2].

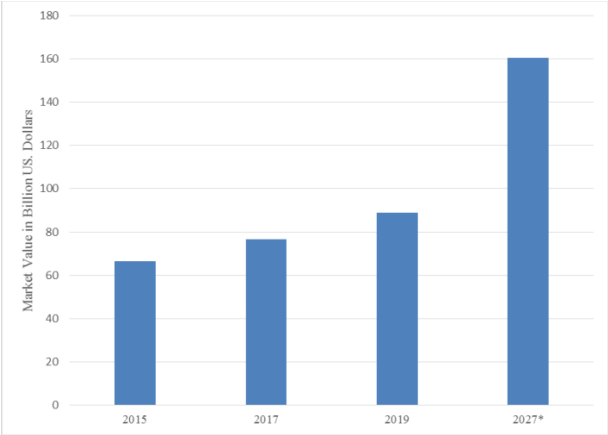

Figure 1. 2: Market value of composite materials worldwide from 2015 to 2027 [2]

Composites are made of reinforcement fibers such as carbon, glass, Kevlar, etc., bonded together in a matrix that can provide high strength, stiffness to weight ratio for the material. Besides, they exhibit a higher fatigue resistance, better stability, lower thermal expansion coefficient, and excellent corrosion resistance; hence they could be a proper substitution of metals in industry. Since fibers usually tend to take random orientation, the matrix aligns the fibers straight. Moreover, it transfers load between the fibers. A variety of composites could be made through a combination of fibers and matrices through different material configurations and manufacturing methods. A good bonding between components, a good amount of fiber volume fracture, and proper matrix curing should be considered to achieve a high-quality composite part with good mechanical and chemical properties.

Based on the structural parameter and the manufacturing constrain of the part, some techniques were developed. For example, for making components with the cylindrical shape or constant cross-section, filament winding and pultrusion methods were utilized. The hand/wet layup method would be suitable for manufacturing the components with simple geometry, usually flat. In this process, the reinforcement was placed manually. The resin rolled over the fibers to wet the fibers and remove the void between each layer partially. Although this technique would limit tailoring, it is still considered one of the cheapest manufacturing methods. Resin transfer molding (RTM) and infusion are two approaches that can drive the resin through the fiber by using a pump and vacuum pressure, respectively. The proposed method's objective is to reduce the cycle time of manufacturing by producing high-volume small parts simultaneously. Automated fiber placement (AFP) and Automated tape layup (ATL) are two novel and intelligent manufacturing methods in the composite industry. This advanced technology was invented thanks to automated technology which is currently in high demand, especially in the aerospace and automotive industries. In this method, the robotic arm is performing the layup to imitate the traditional hand layup technique by stacking the laminas on the mold. This idea has significantly served the concept of fabrication of largescale parts. In AFP, the prepreg strip width is usually designed as 3.2, 6.4, or 12.7mm. In ATL, this value is determined as 75 to 300mm indeed leads to higher productivity, especially for larger but non-complex structures. To describe the fiber deposition with this method, firstly, the fibers are transferred through fiber delivery system known as a feeding unit to the spool head by controlled feeding rate. Tows are laid down by the compaction of the roller while heated at the head or during the delivery to assure perfect cohesion to the stack. Hot gas torch supplied with nitrogen gas wieldy used as a heating element to prevent any oxidation at high temperature. At

last, the tapes are cut using knife-edge or more complicated equipment such as a laser. Higher quality, higher productivity, and remarkable reduction in the labor force are some of the main benefits of this novel principle compared to the usual techniques. In addition, the agility of the method would satisfy the layup process even in a more complex manner, which means that this phenomenon can be done while the robotic arms are steering to have a more flexible design in order to reach the desired fiber orientations. More novel approaches were followed nowadays, inspired by 3D printing technology to merge the automation and composite layups at a much smaller scale. This domain is still in its early stage and requires more attention. Despite all of the advantages mentioned above, there are some restrictions regarding these methods. For instance, in the AFP method, the complexity of the parts and the process parameters such as temperature, feed speed, compaction force, fiber tension, and steering radius play an essential role in determining the quality of the fabricated part. Still, the bright point is that since the machine is equipped with several sensors, observing and controlling the components is facile. Furthermore, the most common defects observed during tow steering are gaps/overlaps between adjacent tows and out-of-plane wrinkles [3] Figure 1.3. Thus, figuring out the fundamentals of the effective process parameters and the nature of mechanical properties of the tow while it is in an uncured state is crucial to predict the possible defect and prevent iterating more experiments.

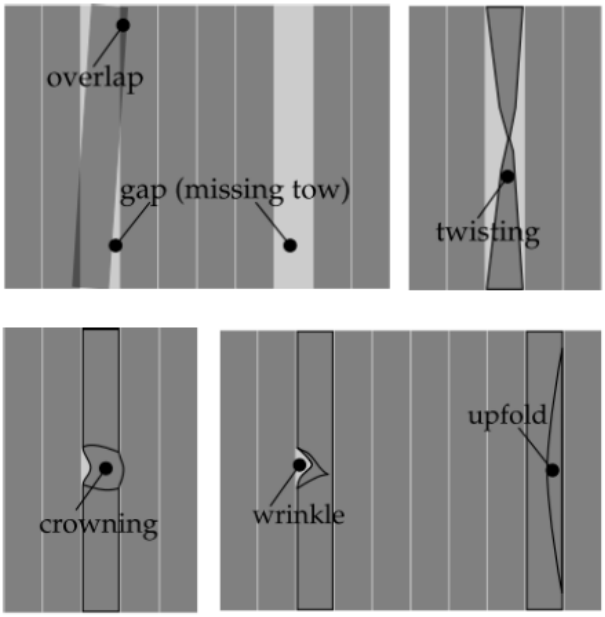

Figure 1. 3: Types of defect found in AFP & ATL during tow placement [3]

A significant number of researches were accomplished to address the challenges in optimizing the process parameters to obtain the radius that comes with the minimum defects.[4][5]**.** The prepreg

tack originated from viscoelastic behavior is considered one of the determinant elements in finding the critical steering radius for securing flawless layup. Since this parameter is highly dependent on other process parameters, obtaining the optimum values is time-consuming and relatively expensive [3]. Some modeling was proposed for a better conception of the physics of the problem [6]. [7]–[9] present their modeling approach to the formation of wrinkles that occur due to the buckling of the settled plate subjected to in-plane loading. [10] has observed the relations of the process parameters with respect to the type of defect in seven cases. His experiments were performed by an AFP robotic arm named XTP-500, which is capable of laying up both thermoset and thermoplastic materials.

	Steering Radius (*mm*)	Nitrogen Gas		Head Speed (*mm/s*)	Compaction Force (*N*)	Defect Type
		Temperature (℃)	Flow Rate (*lit/s*)			
1	889	250	75	114	222.4	No Defect
2	635	220	100	88	266.9	In-Plane Waviness
3	635	220	100	76	266.9	Sheared Fiber
4	558.8	250	75	114	311.4	Tow Pull up
5	558.8	250	75	114	222.4	Wrinkle and Blister
6	558.8	260	85	140	222.4	
7	558.8	250	75	114	111.2	No stick

Table 1. 1: Evaluation of process Parameters in AFP resulting in different layup quality [10]

The alternative way that is also the main interest of this research is fabricating the part in a flat configuration. The laminates are laid down by machine or hand layup then subjected to forming process. Compression molding has the benefit of producing small composite components with more complex geometry. This method functions similarly to metal casting. In this method, the composite part is inserted into the empty space of the molds, and then the molds are loaded mainly so that the piece can be cured under the provided high temperature and pressure. Double-diaphragm forming can reduce the cost of the previous method. It has high efficiency and productivity during forming. It consists of three steps. First, the area between the diaphragms is subjected to vacuum then the part is placed between them while heated up. At last, the vacuum is applied in a controlled manner to make the deformation according to the stencil forming box, making the complex contour shape is possible through this technique. These approaches can significantly minimize the restriction of spool steering, but instead, Several deformation mechanisms forming such as intraply shear, interplay friction, tensile and out of plane bending are

happening during the forming, therefore, to precisely predict the defects which are primarily emerged as wrinkling, the knowledge of deformation under different processing condition are needed. Among different composite reinforcement architecture, textile attracts lots of attention it has better impact behavior, and importantly it is more droppable compared to other fibers configurations.

Minimizing the defect in composite parts is of great interest. Among the deforming mechanisms, bending stiffness highly affects the amount and size of wrinkling. The bending stiffness of dry fiber or uncured ply is much less than the cured one, and also, applying pure bending is difficult. At present, there is no accurate modeling that can consider every aspect to predict the bending stiffness. So, understanding the fundamentals of bending behavior is still challenging and requires more work. In this study, the experimental and theoretical approach is investigated and compared, and at last, the finite element simulation is implemented to verify the outcomes.

1.2 Aims and objective

Nowadays, the demand for composite material due to its excellent mechanical features is increasing. Hence, coming up with an optimized manufacturing method is crucial to satisfy both the productivity and cost-effectiveness of the final product. Automated manufacturing such as ATL and AFP can roughly resolve the needs because of its limiting factor in producing complex geometry. To overcome these limits and obtain the optimum technique with the highest productivity, it was recommended to break down the process into three stages instead of forming the component in a single step. Firstly, the two dimensional flat laminate is laid down by automated systems, then the forming takes place, finally, the parts are cured. This procedure would decrease the cost considerably and eliminate the manufacturing restriction of automated methods. In this approach, the forming is carried out when the material is in the uncured state, so all the deformation mechanisms take place at this state.

Furthermore, there is significant variability in material properties between cured and uncured states. So this matter might make it challenging for manufacturing and defect prediction. Thereby, more research needs to be done even though many studies have been fulfilled in this area. Until now, many researchers have proposed a variety of attitudes to characterize the bending behavior of prepreg composite. But still, there is no precise theoretical model to embrace all the effective parameters and reveal their influence in predicting the bending stiffness. Consequently, the main

objective of this thesis is to address one of the essential elements known as viscoelasticity in determining bending characteristics during the process. The idea aims to minimize the knowledge gap concerning the bending behavior of uncured carbon fiber used in the forming. The approach is implemented as the following:

(1) Obtain the viscoelastic properties and their dependency on other physical parameters through the experimental investigation.
(2) Develop a mathematical model to define the viscoelastic behavior of uncured prepreg and utilize the model for deriving the governing equation for bending
(3) Implement the forming mechanism in the ABAQUS environment in order to demonstrate the correlation between modeling and finite element

The result of this study will be applicable to the forming process to reduce the possible defect prior to manufacturing the real part.

1.3 Thesis outline

The present thesis is divided into 6 Main sections. In the beginning section (Chapter 1), a general introduction of composite material and its forming process are outlined. In addition, the physical phenomena occurring during the forming are mentioned, and the types of possible failure are discussed. The motivation of our study is also described. Chapters 2 brings a summary of the previous studies. This section mentions the accomplishments and the proposed solutions. Also, the current challenges that were not covered by other researchers are addressed. In chapter 3, the characteristics of the material that will be used are presented. The test procedure required equipment and methodology are defined. Also, the effect of temperature in predicting the viscoelastic features is focused. In chapter 4, different approaches in mathematical modeling of the viscoelastic properties of uncured prepreg were mentioned and compared. In the following chapter, the constitutive bending equations are derived for the material by taking into account the viscoelastic parameters. Chapter 5 provides a summary of the finite element approach and its importance in predicting the defect during composite forming. Afterward, the experimental observations are verified in the ABAQUS platform. The last section of the thesis (Chapter 6) brings a comprehensive statement of the goal and thesis achievement. Finally, future works are recommended, and the remaining challenges are addressed.

2 Literature Review

A good portion of literature has been dedicated to studying the deformation mechanism when the composite is subjected to the forming process either in dry fiber or prepreg. These works result in a better prediction of the potential defect formation. interply slip exists when there is a multiple laminate stack. This mechanism refers to the ply-ply friction or tool interaction causing friction that releases compressive stress may create buckling. Extensive research indicates that layup configuration, pressure, temperature, and slip velocity are the effective parameters of this kind of mechanism [11][12][13]. As it was mentioned earlier, during the forming process, the sample was under gone several deformation mechanisms (tensile, in-place shear, and bending stiffness). In the following section, some related studies that have been implemented in each domain were presented.

2.1 Review of mechanical properties related to forming mechanism

In textile fiber architecture, intraply shear plays a primary role during the forming since it allows the composite to obtain complex curvature. The degree of this mechanism is measured by the angle of the rotation of the yarn at their intersection. B. Zhu et al. [14] Mainly focused on pure shear deformation. The contribution to wrinkling and the effect of test conditions like reduction of yarn width was investigated through the modified picture frame test method to show the wrinkling occurs in critical shear angle. Gilbert et al. [15] presented their efforts in predicting the forming process by testing the intraply shear test on polypropylene/glass fabric with two different methods called Bias extension and picture frame testing and also the modified version of picture frame test was developed in his work to minimize the related difficulties such as unwanted excessive tensile load.

P. Boisse et al. [16] simulated textile composite reinforcement forming based on a simplified form of virtual internal work. It was concluded that the wrinkling formation depends on all strains and stiffness as well as boundary conditions, and it was noted that bending stiffness is the main factor in determining wrinkles. P. Harrison [17] proposed a normalization procedure with respect to sample length for bias extension testing, which allows the Bias and frame results to be compared. Each method has its pros and cons, which was stated in table 2.1

	Picture Frame	Bias Extension
Pros	➢ Easy to perform ➢ Shear angle can be derived from displacement ➢ Homogenous deformation throughout the sample ➢ Can control shear rate during test	➢ Easy to perform ➢ Convenient way to measure locking angle ➢ Results are less susceptible to non-uniform temperature field
Cons	➢ Need specialized rig ➢ Problems with sample alignment ➢ Clamping option may affect the result ➢ Metal clamps may induce non-uniform temperature field	➢ Need specialized clamping grips ➢ Heterogeneous deformation in sample ➢ Need to mark sample and image analysis to measure shear angle ➢ Range of shear angle is limited ➢ Difficult to control shear rate

Table 2. 1: Advantage and disadvantages of the picture frame and bias extension test [17]

E. Guzman [18] studied the viscoelastic behavior of prepreg thermoplastic using the Bias extension technique and proposed a model to simulate the forming process at a macroscopic level based on hyper elastic behavior coming with dry fiber approach. The simulation performed in this literature has shown that the in-plane shear stiffness increases so as wrinkling formation for a high strain rate in low temperature. I.Taha [19] investigated the shear behavior of natural fibers with plain weave architecture and various areal densities to describe the shear characteristics such as shear force, shear angle, and shear lock angle. Rahul [20] studied the shear behavior of out-of-autoclave carbon/epoxy used in the diaphragm forming process at different temperatures and loading rates. It was concluded that as the temperature increases, on the other hand, viscosity decreases. So that results in delays in the interlocking points of the yarns, i.e., postponing the emerging defects. Digital Image Correlation was utilized to depict the deformation stages and capture the onset of wrinkling formation.

One of the rudimentary mechanical properties of any material is tensile behavior. To achieve a precise model for forming simulation, this characteristic must be comprehensively recognized. Either during AFP or ATL process, where the robotic arm is steering to place down the layup, or compression forming with certain die or mold's boundary condition, the prepreg would face the uniaxial tensile force. Insufficient tensile force can result in unwanted defects. Some studies have been conducted to investigate the tensile properties of uncured prepreg.

K.potter et al. [21] investigated the tensile properties of uncured prepreg at a different range of temperatures. They addressed the effect of fiber waviness in determining this modulus. In their test setup, the end of the sample had an extra layer, and during the test, the ends were cured rapidly to minimize the slippage. They also illustrated that the stress-strain plot consists of a linear and nonlinear region.

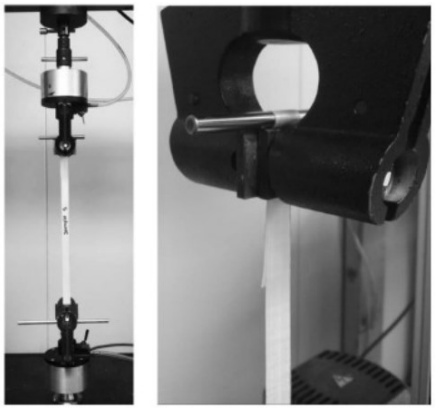

Figure 2. 1: External pins proposed for gripping solution [22]

W. Zhang [23] performed a uniaxial test on uncured woven composite. In their test setup, Digital Image Correlation (DIC) was utilized to acquire the deformation strain. Tested was conducted between the temperature range of 3 to 80℃. Similar to [21], to prevent slippage, the ends of the samples were partially cured, and stress-strain was depicted. Dangora et al. [22] proposed a new solution to suppress the gripping difficulties for testing uncured cross-ply thermoplastic prepreg by incorporating external pins in which the sample ends were wrapped around Figure 2.1. The temperature dependency of tensile properties was also expressed using a ceramic heating plate subjected to the sample face. They concluded that since the temperature rises, the polymer's chains movement is facilitated, which results in declining the stiffness of the material Figure 2.2.

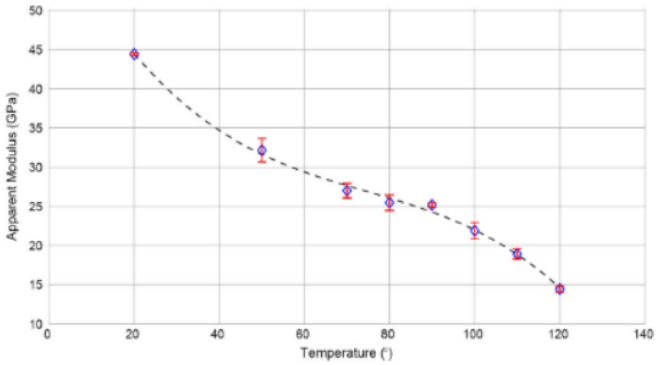

Figure 2. 2: Tensile modulus of thermoplastic cross-ply lamina versus temperature [22]

As previously stated, the bending behavior of the composite reinforcement becomes a necessary behavior that needs to be considered while forming is modeled. This leads to several studies. Pierce [24][25][26] and Wei [27] designed a test method to derive the bending stiffness of the dry fabric.

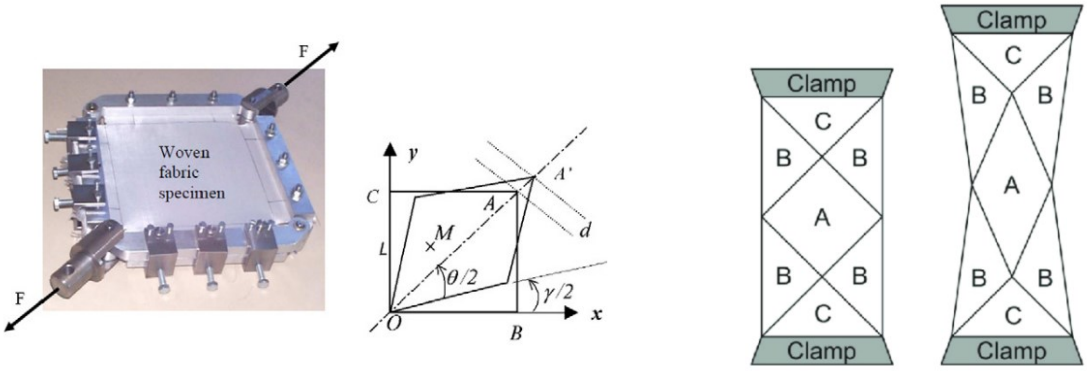

(a) (b)

Figure 2. 3: (a)Picture Frame Test (b) Bias Extension Test [16]

In the test, the sample drops under its own weight, and the angle was measured. Following the different mathematical approaches, the bending rigidity was obtained through equations 2.1 and 2.2. In these methods, the sample was prepared in a rectangular shape and placed into the setup named Flexometer shown in Figure 2.4. The sample was assumed as a horizontal cantilever beam. These approaches have studied the linear elastic behavior of fabric.

θ	10°	20°	30°	40°	45°	50°	60°	70°	80°
$\frac{\cos\theta}{8\theta}$ [26] (2.1)	0.705	0.337	0.207	0.137	0.113	0.092	0.060	0.035	0.016
$\frac{\cos\left(\frac{\theta}{2}\right)}{8\tan\theta}$ [27] (2.2)	0.706	0.338	0.209	0.140	0.115	0.095	0.063	0.037	0.017

Table 2. 2: Comparison of Equation 2.1 & 2.2

J denotes flexural rigidity per unit width, l is overhang length of the strip, θ indicates the angle of the bending, and w is known as weight per unit length.

Table 2.2 indicates the difference of trigonometry terms of two formulations for various bending angles, and it was shown that the obtained values are almost the same. Furthermore, [26] claimed that according to the sensitivity analysis of the proposed formula compared to experimental observations, θ = 53 provides the best accuracy for the definition of flexural rigidity.

Since the sample was kept horizontally in these techniques, the twist may occur during the test that doesn't produce pure bending. So the positioning of the sample needs great attention. It was also concluded that, unlike continuous materials, textile's and composites' out-of-plane properties could not be derived from in-plane properties.

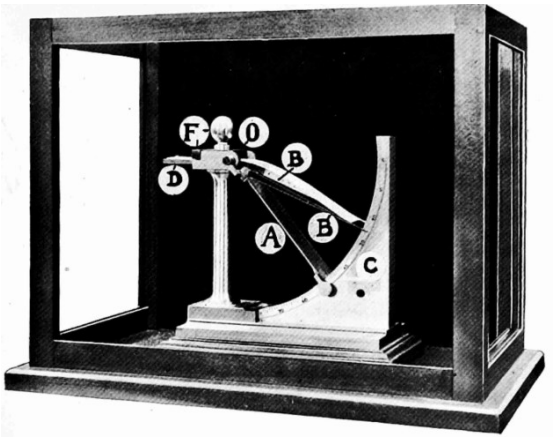

Figure 2. 4: Flexometer Apparatus

Bilbao [28] used a flexometer with an optical measurement device that can carry out a set of cantilever tests under different load cases and bending lengths to show the nonlinear non-elastic behavior of reinforcement bending. This study also mentioned that the bending model proposed for clothing textile is not suitable for composites reinforcement due to the types of loading and material constitution. It was also recommended to discover the related and effective parameters by doing more experimental and finite element analysis.

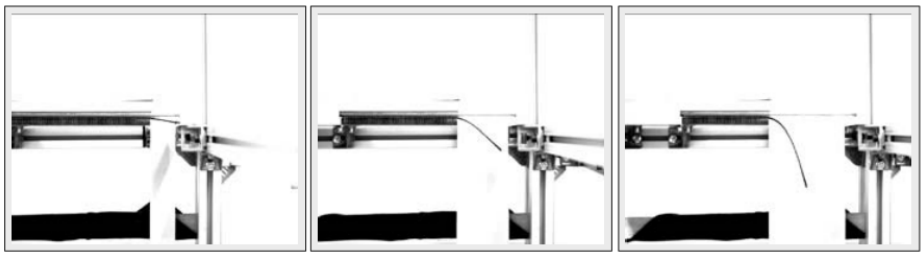

Figure 2. 5: Bending length measured using optical module [28]

Liang [29] developed an experimental approach based on cantilever beam deflecting both under its own weight and added mass. In addition, the effect of temperature in the forming process was discussed because it has a direct relation to resin viscosity, but the impact of viscoelastic was out of its scope. To see the temperature effect, the test was set up and compared for two materials (PEEK-carbon and PPS-carbon satin prepreg) in an environmental chamber with temperature and humidity control capability. As the temperature increases, the deflection increases significantly until a point at which the resin melts entirely, and the fabric entirely determines the bending stiffness. Based on the measured bending stiffness, simulations of thermoforming were performed. The amount of bending stiffness at the manufacturing temperature is important as it establishes the size of the wrinkles Figure 2.6.

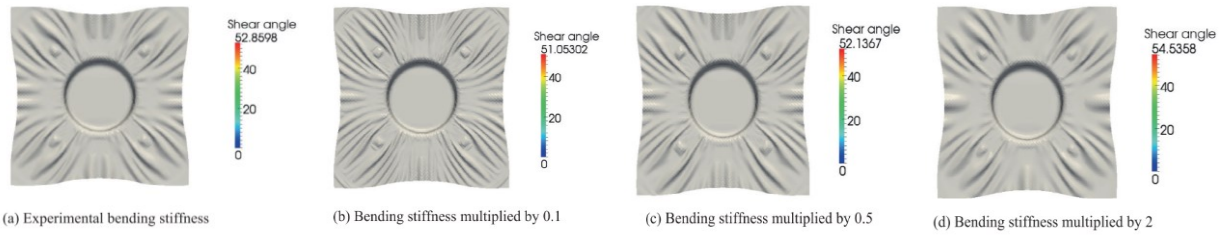

(a) Experimental bending stiffness (b) Bending stiffness multiplied by 0.1 (c) Bending stiffness multiplied by 0.5 (d) Bending stiffness multiplied by 2

Figure 2. 6: The effect of bending stiffness in determining the size of wrinkle [29]

D. Soteropoulos [30] governed the bending stiffness of biaxial non-crimp fabric (NCF) because this material was chosen due to its superiority in the absence of undulation in comparison to the regular fabric. In their approach, the sample test was placed vertically to avoid any potential twist and loaded to the desired displacement using mass and spring. The digital analytical technique was implemented to capture the deformed shape then the digital image results were combined with the proposed finite element model to determine the bending rigidity of the fabric through an iterative manner.

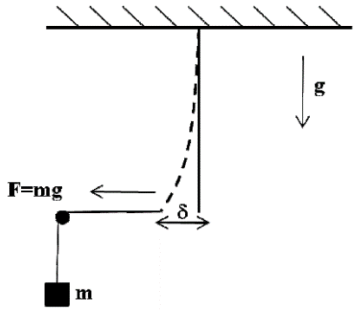

Figure 2. 7: Schematic test setup of the system of vertical sample attached to mass[30]

Dangora [31] investigated characteristics of temperate dependent of tensile and bending rigidity. Due to probable slippage between sample and holder, a modification to the standard test method was implemented, and a longer gauge length was used. The bending test was developed based on a vertical cantilever beam at elevated temperature, and results were used in a finite element model which was using hybrid discrete mesoscopic approach; and at last, the capability of the proposed model was measured with deep-draw forming simulation.

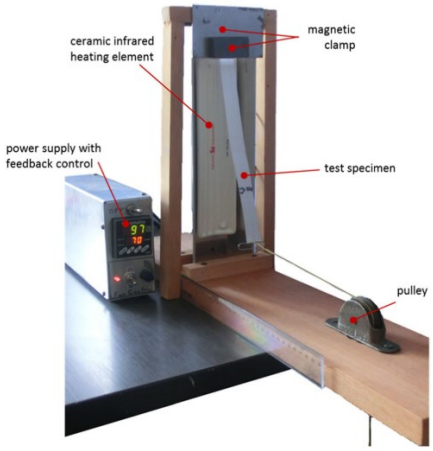

Figure 2. 8: Test setup for evaluation of bending stiffness at elevated temperatures based on the vertical cantilever method [31]

Lomov [32] studied the deformability of multiaxial multiply fabrics. Kawabata Evaluation System (KES) [33] was utilized in their experiment to evaluate the tension, shear, bending, and friction characteristic. Specifically, in bending test the circular path loading was applied to the specimen in order to ensure pure bending. In the KES testing system, the load regime is low, and the pros of this test are that it is time-consuming and expensive.

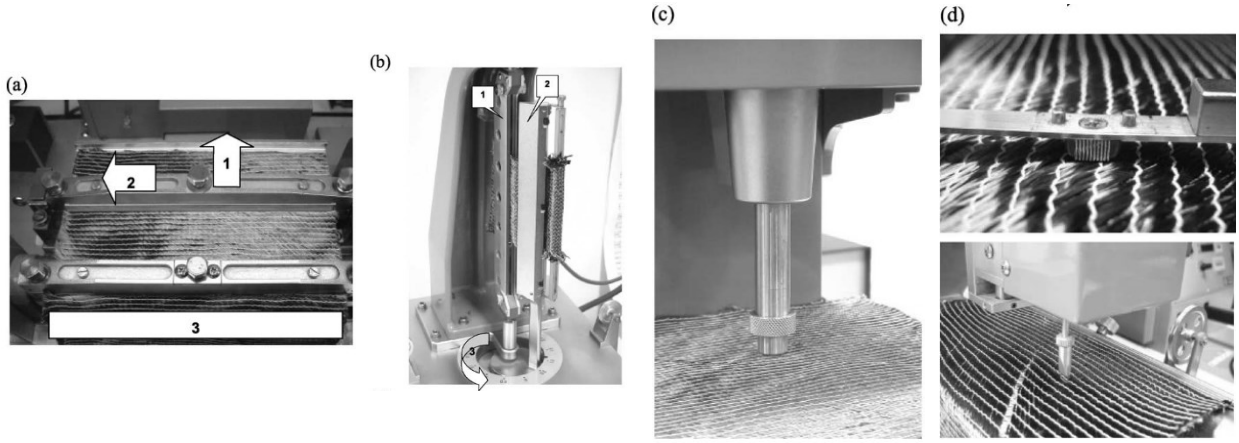

Figure 2. 9: KES test setup for measuring (a) Tension and shear (b) bending (c) compression (d) surface friction coefficient and roughness of multiaxial multiply fabrics

Martin [34] investigated the forming process characteristics of Carbon fiber/Polypropylene composite using three-point bending with V shape punch at elevated temperature. In addition to the temperature effect, the shape of the strip as it forms and the influence of forming speed was presented. At last, the obtained results were compared with the proposed analytical modeling. This method allows inter-laminar shear to be deboned from bending to be analyzed individually. 3-point bending requires large bending stiffness so it could be applicable for consolidated fibers or thick dry fabrics, otherwise, motion is not controllable.

Wang [35] mainly focused on the bending deformation mechanism. The experiment procedure was developed based on large displacement buckling to investigate the viscoelastic aspect and show the bending behavior depends on bending displacement rate and temperature. One of the main advantages of this method is that the applying load is much easier than another bending test method; however, the prepared sample test for this test is small.

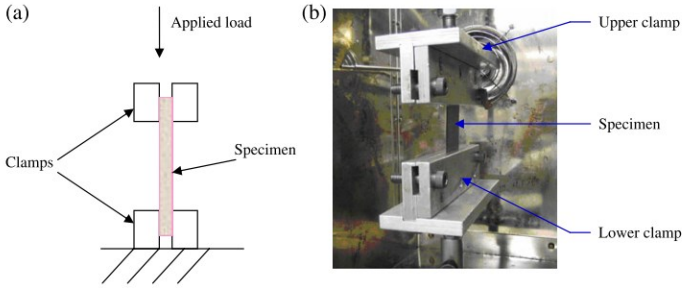

Figure 2. 10: Representation of (a) schematic layup (b) experimental setup of buckling test [35]

Margossian [36] proposed a new test method using a dynamic mechanical analysis (DMA) system to define out-of-plane bending properties of the unidirectional thermoplastic composite. Several specimens with different geometry placed in various test fixture was studied to show the temperature and displacement rate dependency.

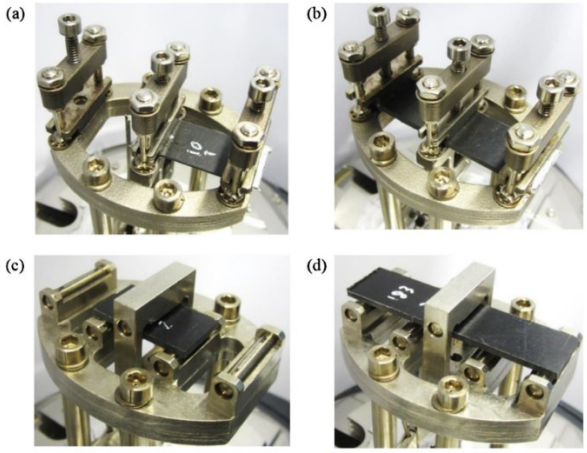

Figure 2. 11: Composite sample mounted on different DMA test fixture (a) single cantilever (b) double cantilever (c) three-point bending (shorter span) (d) three-point bending (longer span) [36]

Ropers [37] used a combination of dynamic mechanical analysis (DMA) and rheometer bending tests to illustrate temperature dependency and viscoelastic behavior. Also, They proposed a linear viscoelastic model and show rheometer can explain the bending behavior of prepreg is nonlinear.

Alshahrani [38] developed a new test method in which the sample was held vertically, and the effect of loading rate, temperature, and viscoelastic behavior was discussed. In this method, the load is applied horizontally to the edge of the sample and controlled by a linear actuator which is

recorded by a miniature loadcell. The sample provided in the test is woven-fabric out-of-autoclave prepreg. The specimen subjected to the heat using an infrared heater and IR camera was used to derive the temperature gradient. A digital camera captured the bent shape, and the data point of the deflection was processed in ImageJ fitted with a polynomial function.

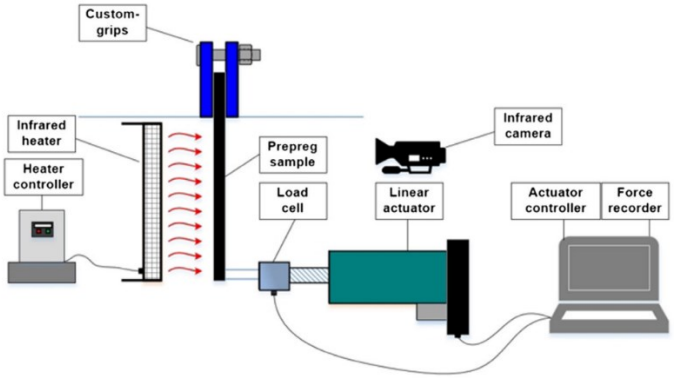

Figure 2. 12: Schematic bending test of vertical prepreg sample [38]

R. Sourki [39] used a customized setup to investigate the pure nonlinear bending rigidity of the dry fiber in loading and unloading cases with the hysteresis effect. It was shown that there is bilinear relation between bending moment and curvature. They concluded that there is in-plane shear coupling in total bending stiffness. In addition, the effect of initial fiber orientation and other geometrical factors was discussed.

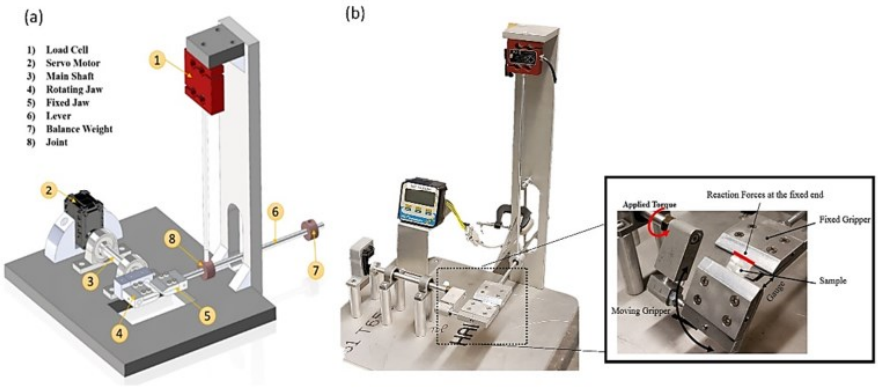

Figure 2. 13: pure bending of woven fabric test setup [39]

Sache [40] conducted an experiment to characterize the bending behavior of UD Carbon Fiber/PA6. In their study, the custom setup consists of a rheometer equipped with a thermal chamber was developed. The sample was bent in a controllable circular path in order to satisfy pure bending. At last, the accuracy of the proposed model provided by the researchers was compared with acquired experimental results.

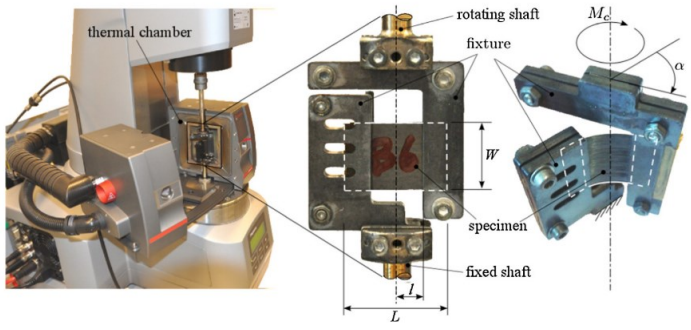

Figure 2. 14: Bending test setup consists of two fixtures which are mounted on the rotational rheometer [40]

2.2 Material Definition

Prepreg has opted as a fundamental constituent in advanced composite manufacturing. This type of composite facilitates parts fabrication in more complicated cases. It is shaped in the form of tape or sheet reinforced by desired fibers architecture impregnated with partially cured resin. The stage of pre-processing known as the B-stage is commonly utilized before shipment. Prepregs can be laid up through conventional or modern methods.

The resins used in prepreg composite are known as polymer materials categorized into thermosetting and thermoplastic subgroups. Thermosetting resins are polymers that are not able to soften after cure by applying heat. In this type, the curing is happening by a crosslinking process in which the covalent bonds between individual chains in the polymer are built as a result of the presence of a curing agent. On the other hand, in thermoplastic material, increasing the temperature causes the polymers chains to lose their intermolecular force transform into the viscous fluid state, in which reshaping can be done quickly. Since the intermolecular chains are pretty long compared to thermosetting material, they have a higher molecular weight.

2.3 Effective Parameters

Physical specifications such as temperature, pressure, and time determine the quality of composite structures defined as void-free, consolidated, and strong laminate. For example, polymer materials are highly temperature-dependent. Thus the modulus of polymers should be measured at different temperatures. It can be realized that the obtained curve for mechanical properties of these kinds of

materials can be segmented into two regions with totally different behaviors. As the temperature is kept low, they behave like glass materials with high modules. However, at elevated temperature, the materials state has been changed, and they are transmitted to a soft rubbery state which exhibits a much lower value corresponds to the modulus. So understanding these dominant parameters and their effect during forming or curing process is crucial to attaining the objective of having intact composite parts.

In general, the thermosetting prepreg is cured in autoclave following a two-stage cycle. In the first stage, the excess resin and trapped gasses are released. Moreover, the resin viscosity remains low while the curing speed slows down to make the resin flows much better in the fabrics network to ensure no dry spot. In the second stage, the higher temperature accelerates the crosslinking process. To degassing the laminate, a constant vacuum is applied until the resin viscosity increases due to crosslinking reaction. Besides, for satisfying better consolidation, continuous pressure is also involved in the whole cure process. [41]

Volumetric changes during cure surely happen when the temperature increases. This phenomenon is rising because of thermal expansions and chemical reactions happening in resin. Since the thermal expansion coefficient of fiber components and resins are different, relative movement happens at their interface, which results in residual stresses. Also, it was shown that as the process proceeds, the direction of the acting force among fibers and resin could change alternately to make it more complex. It is worth to be noted, as the shrinkage of laminate is highly related to the direction of the lamina, despite the benefits of tailor-ability of stacking laminates, due to the mismatch in CTE, the residual stress can be distributed through whole laminates as well. Consequently, to have better control over the curing process to prevent any undesired shrinkage, compromises should be made between the heating/cooling rate. Since during the cure, there is an interaction between the Tooling part and the laminate, the selection of the tool is also important. The thermal coefficient and roughness of the tool are the parameters that define the magnitude of their interactions. [42][43]. In addition, the geometry of the laminate can also affect the part quality. For instance, in thick of complex shape laminates, the temperature cannot be distributed uniformly, which creates spots with different degrees of cures as well as different mechanical properties.

2.4 Viscoelastic

Viscoelastic is defined as a property of materials that shows both viscous and elastic behavior of sample when it was subjected to stress or deformation. In viscous materials like most fluids, deformation is time-dependent and proceeds slowly when the stress is applied. However, the elastic materials return to their initial state as soon as the stress is removed. Viscoelastic is composed of elastic and viscous components; in viscous components, due to the viscosity feature the material shows strain rate dependence in time; also it specified the energy dissipation in the form of heat, usually when the load is applied. The amount of energy is equivalent to the area of the hysteresis formed in stress strain graph during the loading cycle, whereas these features are not.

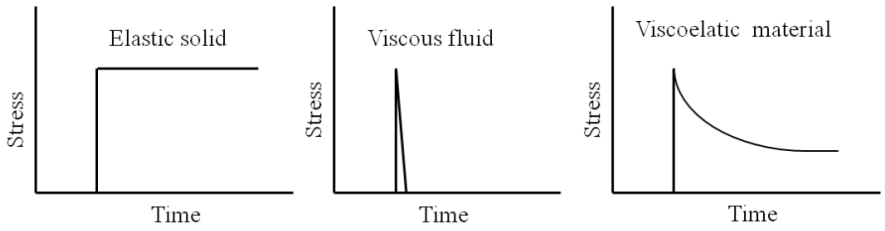

Figure 2. 15: Stress relaxation behavior of elastic, viscous, and viscoelastic materials

defined in the elastic component. Stress relaxation is one of the main fundamental features in describing viscoelastic materials. Stress relaxation is determined when the material is subjected to a constant strain. Because of the nature of viscoelastic materials, the arrangement of the molecules continues to change as a function of time and while stress reduces. Figure 2.15 illustrates the stress relaxation behavior of elastic, viscous, and viscoelastic materials. In elastic material the level of stress remains constant as time goes on. Viscous material dissipates stress instantly and gets back to zero stress level, and for viscoelastic material, stress decays with time.

Several types of research have been presented in the literature to demonstrate a comprehensive understanding of polymer materials' stress relaxation, which is the interpretation of the viscoelastic feature. Kim et al. [44] has shown that the viscoelastic behavior of polymers is highly dependent on the degree of cure. Shrotriya [45] proved the relaxation modulus of laminated depends on not only matrix nature but also the geometry of the fabric configuration may play a significant role. Based on Masuko and Kawai's [46] study, the relaxation properties showed different fiber orientation behaviors. It could be understood that the previously research mainly focus on the relaxation behavior of the polymers in their curing process or fully cured stage. As it was

mentioned earlier the quality of the material is also essential in every step of its preparation to reach the final part.

There is extensive literature that has been performed on the viscoelastic and stress relaxation of polymers. They conducted many experimental and analytical studies to provide a better perception of time-temperature and rate dependence of these sorts of materials during cure or after cure, and their concept was extended in different scales (micro, meso, macro). However, there is still a lack of research in defining the viscoelastic principle of a more complex material like an uncured composite, especially where the fibers and matrix are not bonded together. Each component should be considered individually, and their interaction would play a significant role in defining properties. As claimed before, during composite forming, the forming process happens when the composites are in an uncured or semi-cured state. Hence knowing all the influential parameters are essential for better prediction of any possible defects. Composites materials are categorized as anisotropic materials, so the mechanical behavior of the material is different in each direction. The main objective of our study is to focus on the viscoelastic behavior along fiber direction at a macro scale. Because of not proper bonding between fiber and resin in the uncured state, any tiny force or deformation may decompose composite structure, so that's why the forming process usually carried on in fiber direction.

3 Experimental Testing

This chapter is devoted to describing the experiments for capturing the stress-strain relation of uncured composite. Stress relaxation properties of the sample both in the room and elevated temperature, andthe horizontal bending test of the clamped sample to observe bending behavior will be performed. Also, the material selection was discussed, and some of its physical characteristics were described.

3.1 Sample preparation

The material used in this study is CYCOM 977-2. This material is composed of carbon fiber and epoxy resin prepreg. This is mainly considered a primary material in the aerospace industry. The fiber is unidirectional (UD) 12k HTS-196. The table below presents some properties of this material from the available datasheet [46]. The dimensional parameters should be measured individually based on the material availability and test condition. In addition, the density provided in the datasheet indicates the density of cured resin. We cannot use the same density for our study because the composite density before and after the cure is totally different due to the temperature and compaction operation during the cure process. So in order to find the density of the sample, the following method was carried out. First, a small sample of prepreg strip with constant width through the length was cut from the prepreg spool to the length of 1.5in. Then the thickness and the mass of the tiny sample was measured by micrometer and microgram apparatus Figure 3.1. The measurement was repeated five times. Specifically for the thickness measurement, different sections of sample were measured and averaged to consider any possible non-uniform thickness through the sample. Hopefully, the measurement gave us near numbers with small deviations. The table below summarizes the averaged value of the measured parameters:

Fiber	12K HTS-196
Resin	CYCOM 977-2
Fiber volume fraction	66%
Cured resin density	1.31g/cm^3
Cure temperature	180±5℃

Table 3. 1: CYCOM 977-2 mechanical Characteristics

In order to derive the density for further analysis, we assume that the cross-section of the sample is a rectangle. So by measuring the width, length, thickness, and mass of the sample, the density could be easily found through the below relation:

$$\rho = \frac{m}{lbt} \tag{3.1}$$

ρ is the material density, m is mass of the sample, l is length, b is width, and t represents the thickness.

By calculating the density, the uniform distributed weight per length w can be found as follow.

$$w = \frac{mg}{l} = \frac{\rho g}{bt} \tag{3.2}$$

Mass (m)	0.0547 g
Width (b)	6.35 mm
Length (l)	38.1 mm
Thickness (t)	0.162 mm
Uncured Density (ρ)	1.44 g/cm^3
Weight per length (w)	0.0141 N/m

Table 3. 2: Specimen measured parameters

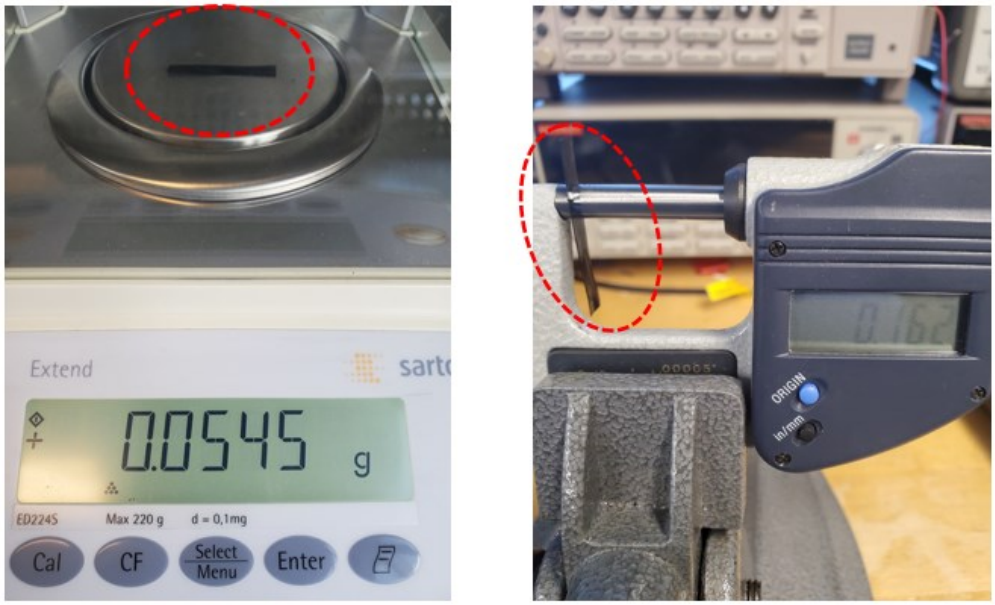

Figure 3. 1: Measured Mass and Thickness

3.2 Test Setup

To perform the uniaxial tensile test, the Hoskin testing machine was used. The load cell suitable for our test was a 1000N installed on the device. Since the sample was not stretched to the failure point, the higher load cell was not necessary. Moreover, when the stress/strain test was performed, it was observed that the initial region of the curve shows a nonlinear response, so using a load cell with a lower capacity would acquire more accurate results. The loading condition is controllable with software linked to the Hoskin test machine; therefore, displacement rate, preload, max load are all adjustable. The standard Knurled grips were used. Since the prepreg sample is not cured, it tends to deform easily, and slippage between the sample and the grips is highly probable. Hence, modification for the grip fixture is necessary. The solution was inspired by Dangora et al. [31], so it was decided to use four bars with a square cross-section. The end of the prepreg strip was wrapped around them, and the bars were joined together two by two using rubbery adhesive tape to secure the sample and minimize any possible movement Figure 3.2. Finally, the whole assembly was placed in the grips of the testing machine. In our experiment, the pin dimension is 6.27mm, and the prepreg total length is 250mm; however, when it was wrapped, the length decreased to 137mm, which is known as the gauge length.

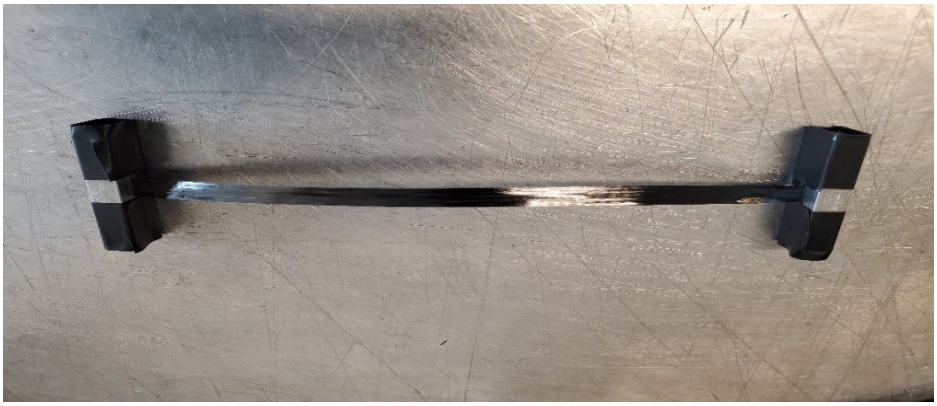

(a)

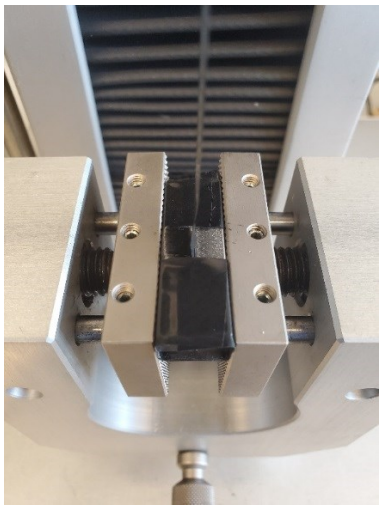

(b)

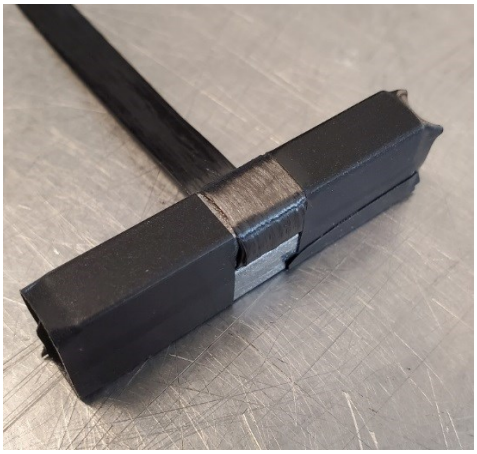

(c)

Figure 3. 2: Picture of sample (a) before mount (b) gripped at machine fixture (c) wrapped around pin bars and reinforced by cohesive tapes

3.3 Relaxation test

Although dynamic mechanical Analysis (DMA) is a technique to characterize the viscoelastic properties of the material, due to the complexity of testing the uncured prepreg, it was decided that the relaxation was implemented by tensile test apparatus. Besides, as the test sample is uncured and highly deformable, it requires special test fixture modification; in a similar study, a film tension fixture was used to implement the test, but the difficulty still makes the experiment complicated. DMA measures not only the stress relaxation but also the dynamic modulus of the material. Because it is capable of applying sinusoidal stress and strain with various ranges of frequency. Also, it is equipped with a special chamber to provide elevated temperature conditions for tested samples to perform temperature analysis. Basically, due to the limitation of the fixture

for our uncured sample, as the temperature rose, the bond between the sample and the fixtures decreased. As it was mentioned in the literature, one possible solution to overcome this problem is that the prepreg partially cured at the ends' locations to provide a better bond, but this method could drastically alter the viscoelastic behavior of the sample.

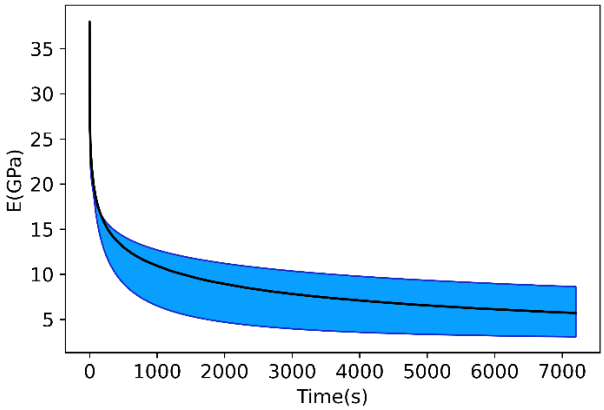

Figure 3. 3: Stress relaxation as a function of time (solid line is average data and the shaded area is data variation)

To implement the relaxation test through tensile machine, the sample was prepared as mentioned in the test setup section. Based on the relaxation theory, the strain should be applied instantly, similar to the step function (Heaviside), so the speed of the head has to be set to its maximum. The strain should be kept constant over the duration of the test. There is indeed no testing machine available to provide instant displacement, so by putting the gauge displacement rate to its highest threshold, 500mm/min, we could diminish the error. The 0.5mm displacement was applied to the sample, and the decaying load was monitored from the load cell over 2hours. The initial stress is due to the elastic response and as time goes on, the stress relaxes due to the viscous effect in the material. The experiment was implemented 5 times to validate the repeatability of the experiment. Figure 3.3, illustrates the relaxation modulus E of the uncured prepreg as a function of time, the averaged value was depicted by solid black line and the shaded area represents the error margin where the boundaries denotes the maximum and minimum values among 5times test implementation.

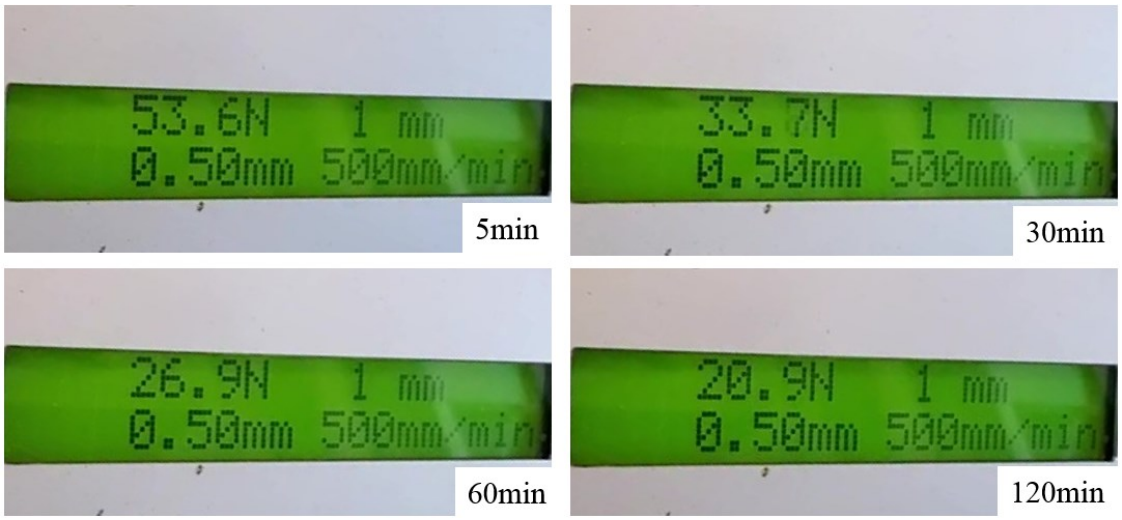

Figure 3. 4: Measurement of relaxed force after 5, 30, 60, and 120 minutes

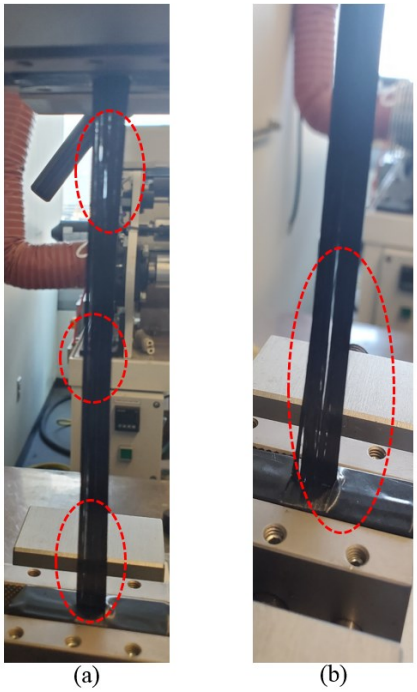

Figure 3. 5: Sample failure at (a) elevated temperature (b) room temperature

3.4 Bending test

The strip of prepreg was cut of 200mm length and placed horizontally in the designed fixture shown in Figure 3.7. The fixture is consists of two separate sections, which have been attached and tightened with two screws. On one of the inner fixture surfaces, a knob was created to fill up gaps between two grips to constrain the sample. This fixture could be considered as a clamped

support that restricts any motion. After placing the sample, the specimen began to deflect due to its weight immediately. So the deflection must be recorded by a camera from the beginning of the experiment. The initial deflection is because of the instant modulus of the sample. As time goes on, the deflection has proceeded. It can be inferred that the deflection is time-dependent. That's why the material's viscoelastic properties are involved for better analyzing the material's bending behavior. In Figure 3.6, the end tip location of the sample, showed by the horizontal dashed red line, gets a lower position as time passes.

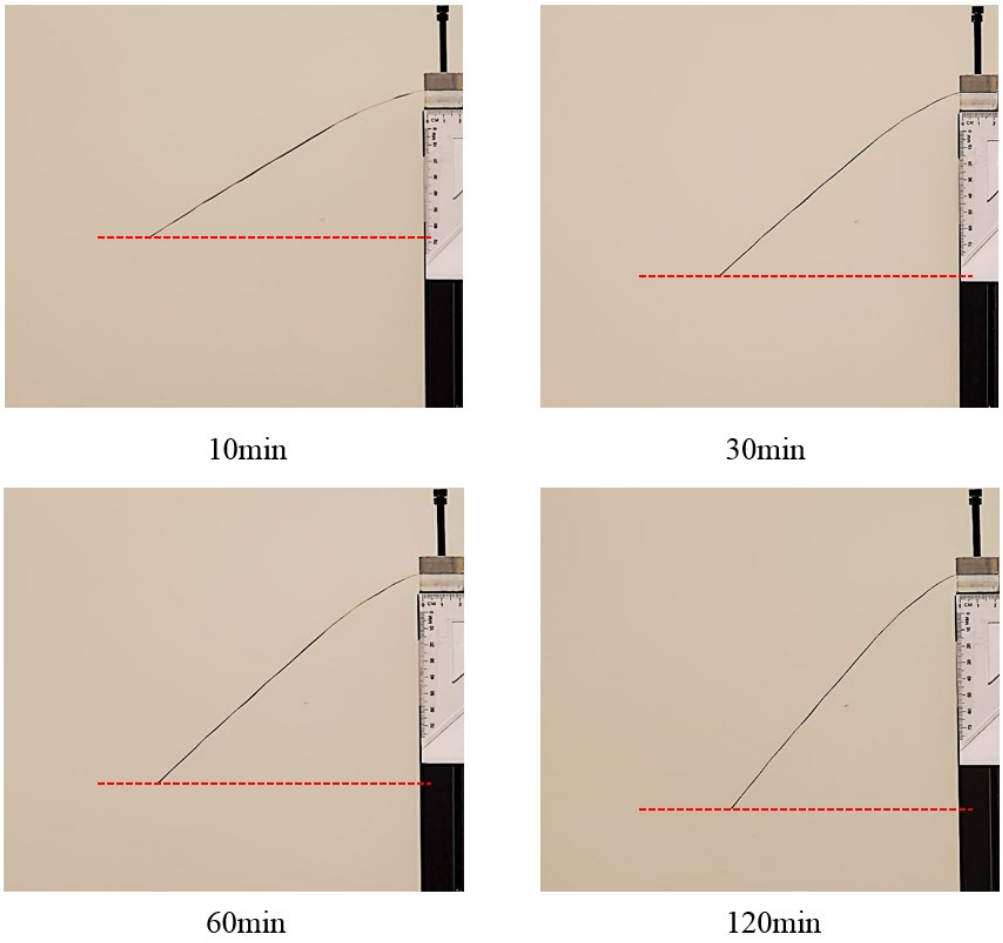

Figure 3. 6: The representation of sample end tip's location

Since the sample was placed horizontally in this test setup, it tends to twist easily, so adjusting the sample requires great attention to guarantee pure bending. On the other hand, the advantage of this approach is that it can properly demonstrate the time dependency of the bending behavior. The deflection points of the deflected sample were discretized into 20 sections, and their coordinates were generated by ImageJ software for different time instants. The Reference point and the scale bar have to be introduced to the software. According to Figure 3.8, point No.1 set to (0,0) as a

reference point and 1cm as a scale bar is defined. Since there is no standard for bending test of uncured prepreg, repeating the test could minimize the uncertainties and validate the accuracy and reliability of the result. So, this experiment was reiterated 5 times, and the x, y average coordinates values were illustrated in Figure 3.9 for 60min time frame.

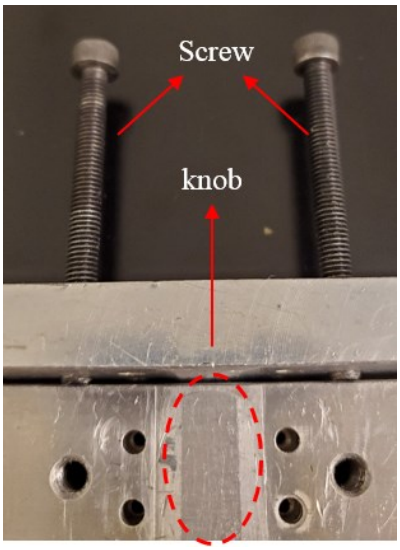

Figure 3. 7: Clamped Fixture Configuration

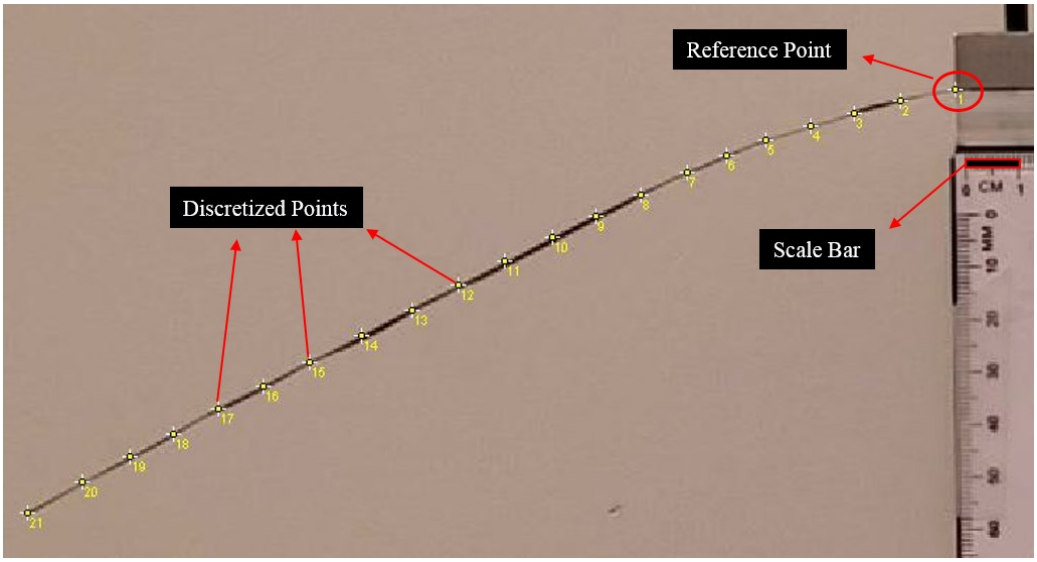

Figure 3. 8: Discretized bending points derived from ImageJ

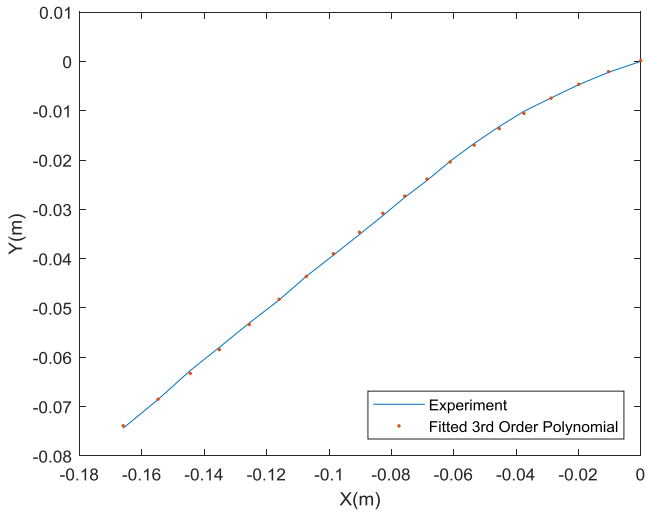

Figure 3. 9: X, Y Coordinates of the bent sample at 60min time instant

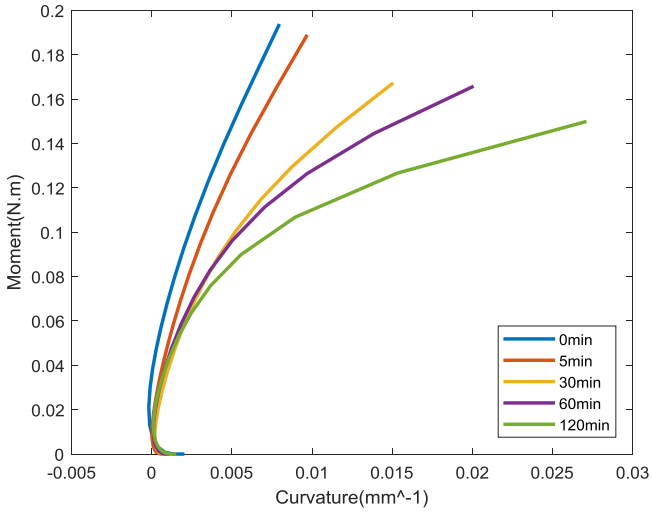

Figure 3. 10: relation of the moment versus curvature at different time instants

Figure 3.10 depicts the relation between bending moment and curvature at different time frames. The approach of deriving this plot will be discussed in detail in the next chapter. The slope of the curve can be defined as the bending stiffness of the sample. It can clearly be seen that the relation of moment and curvature is quite linear for lower time frames (t<5min). However, after a specific time instant, the sample behaves differently, which results in nonlinear relations as the time increases; this nonlinearity will increase. There might be two explanations for this behavior. First, The prepreg material can be cured even at room temperature, so after some minutes, the sample could be partially cured. Moreover, the moment at the fixed end remains high as time goes on the

moment relaxes, so during the test, this relaxation may change the fiber-resin configuration at the micro-level.

3.5 Relaxation test at a higher temperature

As mentioned earlier, the relaxation test was implemented by a tensile test machine. So coming up with a new technique to provide a higher temperature for our test is required. It was decided to select an IR lamp as a heat source. The advantage of the heat lamp is that it doesn't have direct contact with the sample and can provide a uniform temperature; moreover, unlike the heat gun, there is no heat convection to disturb the sample during the test. The location of the lamp was set up on the stand, and the head was placed away from the prepreg to the target temperature. The desired temperature of this study is the sample surface temperature which was observed by FLIR thermal camera. The test should be conducted after letting the sample reach the uniform temperature. In all tests in which the sample was stretched, any misalignment should be corrected by applying initial forces acted as a preload to the sample. The elevated temperature was kept between the ranges of 10 to 20 degrees higher than room temperature (35, 45℃) because the resin has viscous properties, so it begins to flow over the fibers where the temperature is too high, resulting in failure. Figure 3.5 shows that the decomposing of fiber and resin media happens in several sections of the tested sample. After preparing the temperature condition, the sample was subjected to a similar relaxation test described in the previous section. Once again, to validate our experiment, four samples were tested at each temperature.

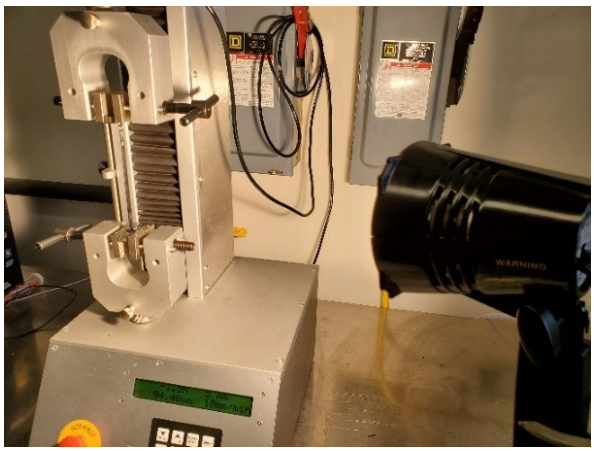

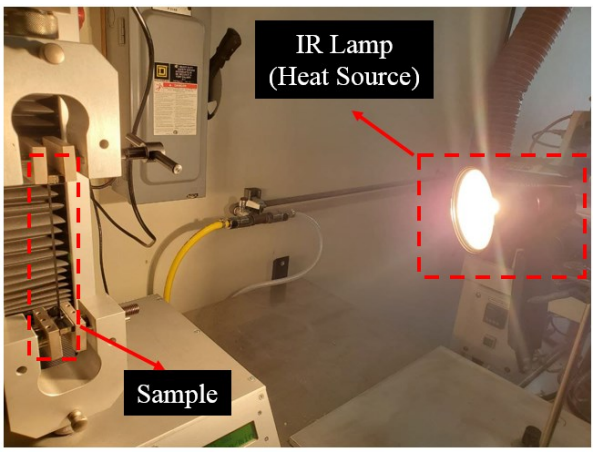

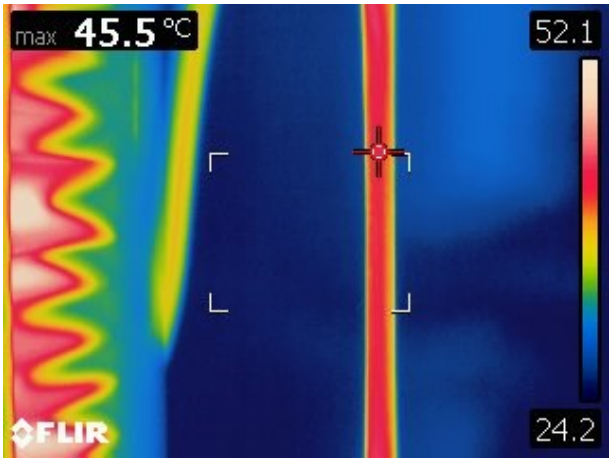

Figure 3. 11: Setup for relaxation testing subjected to higher temperature & uniform surface temperature captured by the thermal camera

As it was mentioned earlier, stress relaxation is time-temperature dependent. The time-temperature superposition principle is a technique to map the response of viscoelastic material at temperature T to the reference temperature T_0 by using the shift factor $a_T(T)$. the concept of this law will be discussed thoroughly in the succeeding chapter. [47] Introduced a methodology and formulation of deriving time-temperature shift factor for polymer composites.

$$\log a_{T_0}(T) = \log(t) - \log(t') \tag{3.3}$$

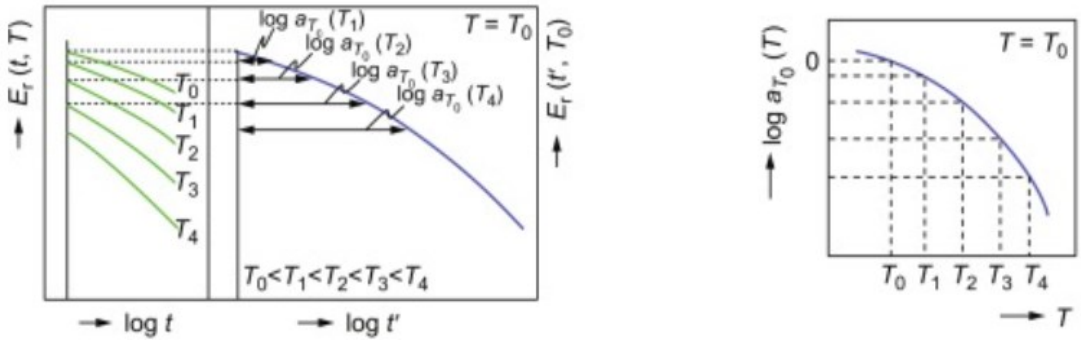

Figure 3. 12: Methodology of shift factor definition [47]

Similar to the given approach, stress relaxation modulus at different temperatures were plotted as a function of time in semi or fully logarithmic scale. The horizontal distance between T and T0 corresponding curves, represents the value of $\log a_{T_0}$. The researches have shown that in linear viscoelastic material, the shape of the curve remains constant regardless of the temperature, and it just duplicated through time with constant distance, however in our experiment, since our material is categorized as a nonlinear viscoelastic material, this statement is not valid. Figure 3.13 shows

that as the stress relaxes, the distance between the curve increases. So it can be concluded that the shift factor is a function of not only temperature but also the current stress value. Figure 3.14 Proves this declaration and $\log a_T$ has been indicated for different force levels.

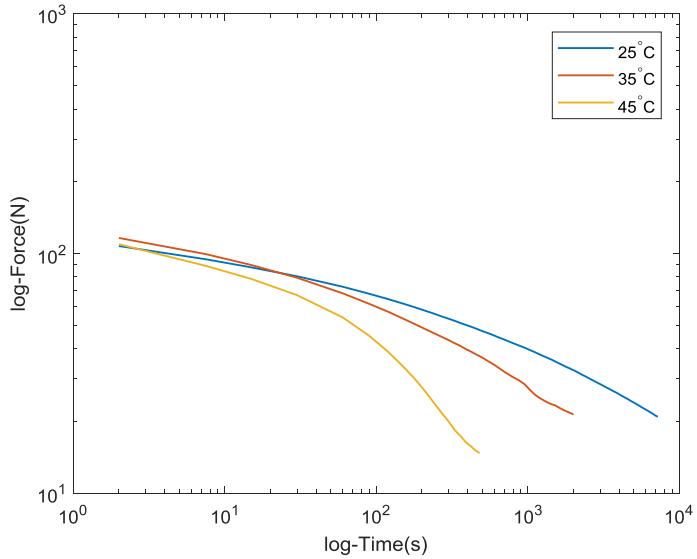

Figure 3. 13: Comparison of stress relaxation value at room and elevated temperature

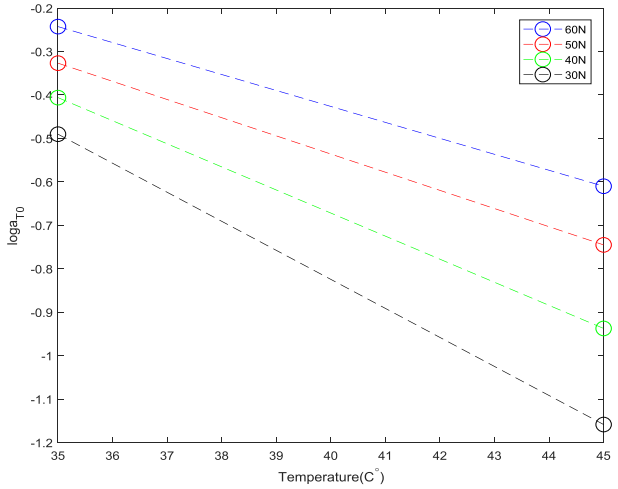

Figure 3. 14: Obtained shift factor for 35, 45℃ at 40,50 and 60N stress level

3.6 Tensile test

The prepreg was mounted on the test machine, similar to the testing condition and sample preparation corresponds to the relaxation test. This time rather than applying the instant

displacement, the grip head moved with the rate of 1mm/s and 2mm/s. The task of applying preload to eliminate twits is also necessary. Unlike the relaxation test in which load variation versus time was the point of interest, the relation of stress with respect to strain was desirable. The principle which was followed to acquire the stress/strain values was that the load captured through the load cell and the distance of moving grips acquired the displacement. The engineering stress and strain can be determined mathematically based on the relation below.

$$\sigma = \frac{F}{b \times t} \tag{3.4}$$

$$\varepsilon = \frac{\Delta L}{L} \tag{3.5}$$

Where σ is the stress along the fiber direction, F is recorded force by loadcell, b and t are the width and thickness of the prepreg respectively, which their value can be found in table 3.2. It is important to mention that the sample begins to fail when the tensile load reaches 200N. The type of observed failure is in the form of decomposition of fiber and matrix where two components are split, as shown in Figure 3.5. Based on the observation, most of the samples were failed around a strain of 0.6%. Since the failure of the sample is not desirable in our study, the test was conducted up to the strain range of 0.45-0.5% to prevent any failure. Because of different fiber waviness in samples, acquired data were highly variant, especially in the nonlinear region, so it is crucial to follow a statistical approach to analyzing the data to omit outliers. Mean and standard deviations are proper tools for this evaluation. Massimo [48] showed that uncured prepreg has a significant variation in mechanical properties with large standard deviations because of the presence of fiber waviness in uncured samples. Therefore, in this study, these variations are depicted by error bars.

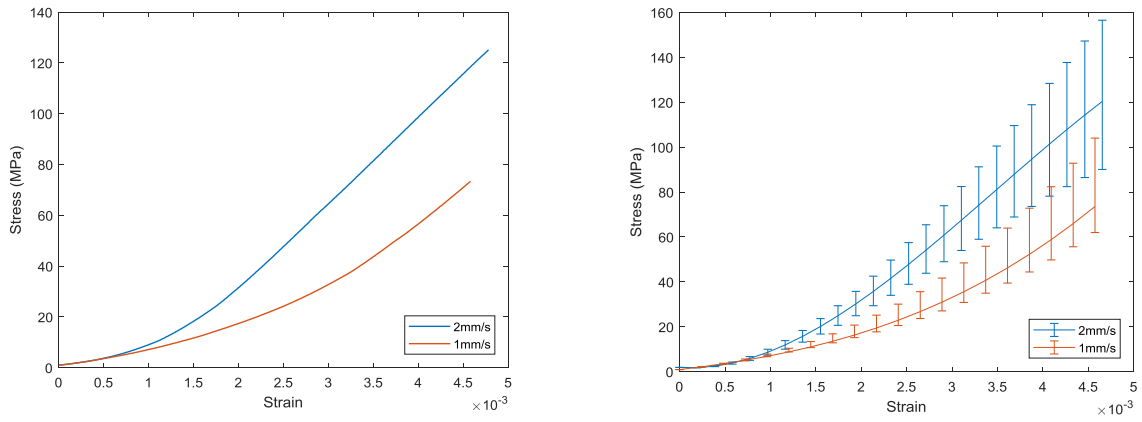

Figure 3. 15: relation of stress versus strain of uncured prepreg at two different displacement rates (a) Average (b) data variation

The stress-strain curve was represented for two deformation rates in Figure 3.15. The pattern of the curve consists of two nonlinear and linear sections. The length of the nonlinear section depends on the deformation rate such that a lower displacement rate results in a more extended nonlinear region. The results of this observation will be used in the upcoming chapter.

As it was mentioned earlier, the preload is always necessary to eliminate twists in the sample. Moreover, while the specimen is initially loaded, the slippage would have been shown by dropping in the force in the plot, if there is any slippage. In order to address the effect of preload in determining the tensile modulus, the sample was initially loaded to 100N, then the force was removed, and it was stretched up to a predefined load before starting the tensile test. The selected preload for this test are 10, 20, 40, 80N. Based on the tensile test observation in Figure 3.17, only a middle portion of the cross-section experiences the load, and the side edges are not in tension. The reduction of the cross-section was measured, and it was 30%. Moreover, the resin in the uncured state doesn't bear any tensile load; as a result, all the load is distributed on the fibers based on volume fraction. Therefore, to define the correct cross-section value in calculating stress, the whole section should be multiplied by the correction factor, which involves the area reduction and fiber volume fraction. Figure 3.16 shows the relation of stress and strain for different amounts of preload after considering the effect of cross-section reduction and fiber volume fraction. The linear section represented the same behavior, and the slope means the tensile modulus.

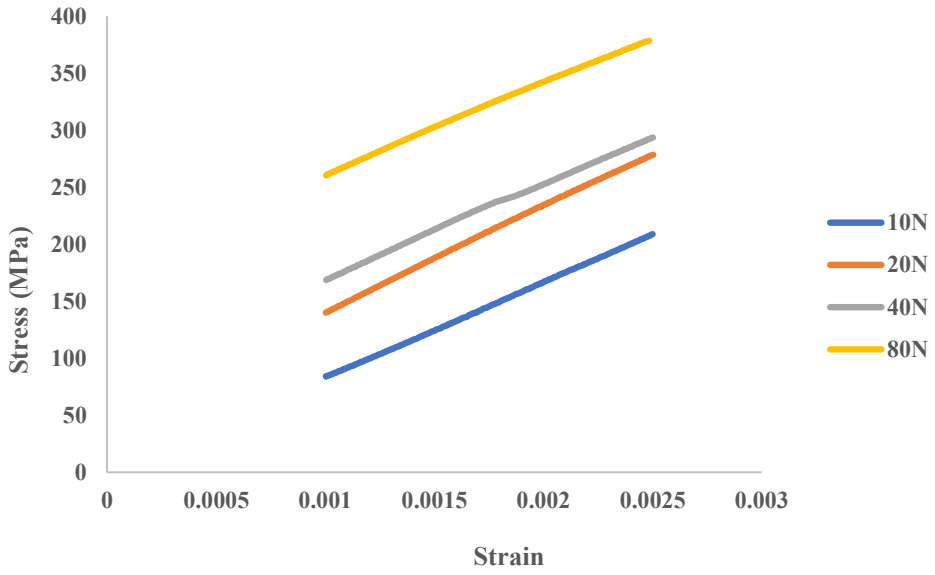

Figure 3. 16: Effect of preload for identification of tensile modulus (After correction)

Table 3.3 represents the slope of the linear section of the tensile test after applying the correction factor. The results indicate that the tensile modulus of uncured prepreg is close to the cured one along the fiber direction. Also, the acquired moduli are in the same range for different preload conditions. The amount of preload cannot significantly affect the tensile modulus; however, a smaller preload can better depict the nonlinear region.

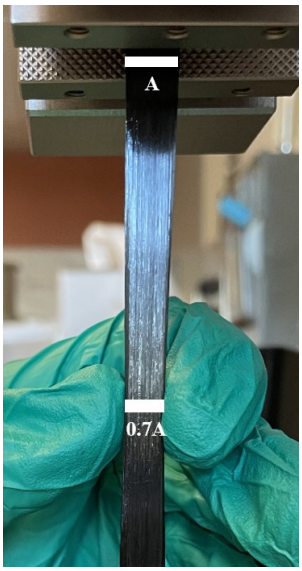

Figure 3. 17: Cross-section reduction

Preload (N)	Slope of the linear section After Correction (GPa)
10	112.512
20	113.084
40	112.378
80	111.325

Table 3. 3: slope of the linear section of the prepreg tensile test subjected to preload

4 Results and Discussion

In this chapter, model representation of viscoelastic material and its contribution to analyzing bending behavior will be presented. The feature of viscoelasticity, same as many other mechanical properties, can be categorized into linear and nonlinear. The simplest form to model viscoelastic material behavior is utilizing the combination of springs and dampers to investigate the relaxation or creep response of these sorts of materials. These models can also be extended by adding more elements. Furthermore, nonlinearity characteristics can be attributed to the linear model by considering the consisting elements as nonlinear elements.

4.1 Model Representation

This section presents the constitutive equations of linear viscoelastic models known as the Zener model, Maxwell model, and Generalized Maxwell or Wiechert model. Afterward, through Inspiring from the Maxwell model and changing the element type, the constitutive model suitable for our case study will be developed.

4.1.1 Zener

Zener model consists of one parallel spring-dashpot and a series spring. It should be noted that in a series configuration, the elements share the same stress, while in the parallel branch, the strain is the same.

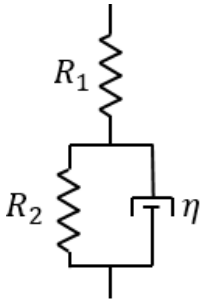

$$\begin{aligned} \varepsilon &= \varepsilon_1 + \varepsilon_2 \\ \sigma &= \varepsilon_1 R_1 \\ \sigma &= \varepsilon_2 R_2 + \dot{\varepsilon} \end{aligned} \tag{4.1}$$

Where R represents spring constant and η denotes viscosity. By taking Laplace transformation, ε_1 and ε_2 were omitted. A simplified equation of the Zener model was obtained in terms of σ, the (^) sign shows the transformed parameter.

$$\hat{\sigma} = \hat{\varepsilon}\frac{R_1R_2 + s\eta R_1}{R_1 + R_2 + s\eta} \tag{4.2}$$

As mentioned earlier, stress relaxation results when the displacement or strain is applied instantly. So, this definition can be represented by modeling the instant strain with the Heaviside function.

$$\varepsilon = \varepsilon_0 H(t), \qquad \hat{\varepsilon} = \frac{\varepsilon_0}{s} \tag{4.3}$$

Then by taking Laplace transformation and substituting 4.3 into the 4.2 model, we will get.

$$\frac{\sigma}{\varepsilon_0} = R_1\frac{R_2 + R_1 e^{-t\left(\frac{R_1+R_2}{\eta}\right)}}{R_1 + R_2} \tag{4.4}$$

4.1.2 Maxwell

Maxwell's model consists of two branches. The Series of spring-dashpot is paralleled with another spring element.

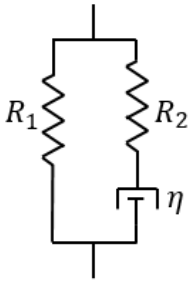

$$\sigma = \sigma_1 + \sigma_2$$
$$\sigma_1 = R_1\varepsilon$$
$$\dot{\quad}$$
$$R_2 \quad \eta \tag{4.5}$$

The presented spring-dashpot system shows the configuration and governing equations of the Maxwell model. Taking Laplace transform and eliminating σ_1, σ_2 for solving $\hat{\sigma}$, will achieve the constitutive equation.

$$\hat{\sigma} = \hat{\varepsilon}\frac{s\eta R_1 + s\eta R_2 + R_1R_2}{s\eta + R_2} \tag{4.6}$$

Plugging in the $\hat{\varepsilon}$ as a Heaviside input in equation 4.6 and taking Laplace inverse, the stress relaxation function was derived.

$$\frac{\sigma}{\varepsilon_0} = R_1 + R_2 e^{-t\left(\frac{R_2}{\eta}\right)} \tag{4.7}$$

4.1.3 Generalized Maxwell (Weichert)

The Generalized Maxwell model or Weichert model is an expansion of the Maxwell model. In this approach, the finite number of series of spring-dashpot are duplicated in parallel with a single spring. Since it has elements arranged in parallel, hence they share the same strain under loading.

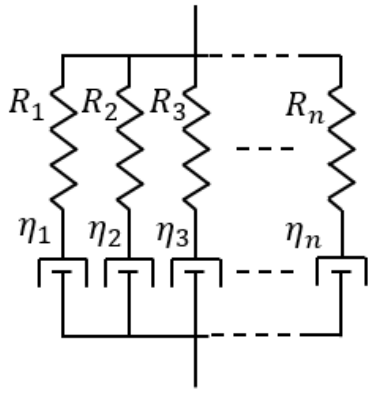

$$\sigma = \sum_{i=1}^{n} \sigma_i \tag{4.8}$$

Where n indicated the number of duplicated units. It was assumed single spring branch modeled with dashpot with infinite viscosity ($\eta_1 = \infty$), so the governing relation of stress-strain is developed as follows

$$\dot{\varepsilon} \quad R_1 \quad \eta_1 \quad R_2 \quad \eta_2 \quad R_3 \quad \eta_3 \quad \cdots \quad R_n \quad \eta_n \tag{4.9}$$

Once again, the stress relaxation function was derived by implementing Laplace transformation and applying the Heaviside strain function following Laplace inversion.

$$\frac{\sigma}{\varepsilon_0} = \sum_{i=1}^{n} R_i e^{-t\left(\frac{R_i}{\eta_i}\right)} \tag{4.10}$$

All the relaxation functions obtained from the mentioned linear model represent the exponential decrease of stress with time.

4.1.4 Prony Model

Pony series is a helpful method to describe the viscoelastic properties of the material in CAE software. The model parameters were adjusted using advanced optimizations to minimize the error between the predicted and data values. Stress relaxation is not only defined for tensile/compression modulus (E) but also can be defined to address shear G and bulk k modulus. Prony series can be expressed as equation 4.11. The terminologies between Prony and GM model are the same, where E_∞, E_i and τ_i in Prony are equivalent to R_1, R_2 and η_i / R_i in GM. E_∞ indicates the long-term modulus when the material is relaxed completely τ_i is the relaxation time, which means that the higher its value, the longer it takes to relax.

$$E(t) = E_\infty + \sum_i E_i e^{-t/\tau_i} \tag{4.11}$$

Prony series is a suitable alternative method to represent the nonlinear model. Figure 4.1 shows that this model can perfectly predict the nonlinearity within the specified time range. The number of elements in prony is defined according to the nonlinearity of the material. It is not true more elements results in more accuracy with a wide range of time coverage. But mainly, higher numbers of elements result in the better fitting. Therefore, the proper number of element always must be found in comparison with the experimental results.

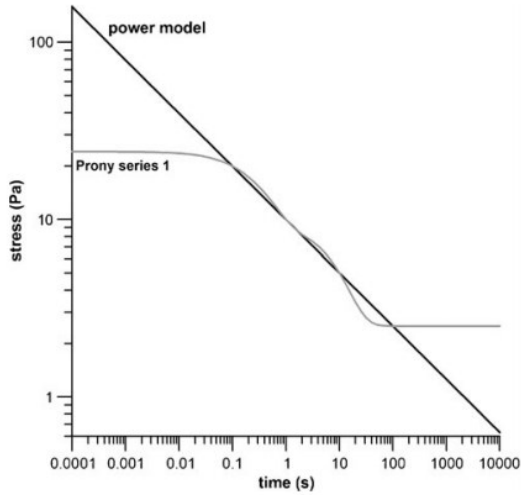

Figure 4. 1: Stress Relaxation of nonlinear model (power) with respect to GM/Prony model[49]

4.1.5 Nonlinear Models

Power law and log law models are characterized as a nonlinear models in which the decay of stress occurs in a logarithmic or power manner. Equations 4.12, 4.13 indicate The constitutive function for these types. When the nonlinear elements (spring or dashpot) are ignored, distinguishing between log or power model doesn't matter.

$$\frac{\sigma}{\varepsilon_0} = R - \eta \ln t \qquad \text{(Log Law)} \tag{4.12}$$

$$\frac{\sigma}{\varepsilon_0} = Rt^{-\eta} \qquad \text{(Power Law)} \tag{4.13}$$

These relations were specified by two parameters R (elasticity constant) and η (viscosity), which have no comprehensive physical explanation like the linear model. Thus, in the following section, the combination of the power-law model with the Maxwell model was proposed for our composite material.

4.2 Detection of Linear and Nonlinear Model

Characterizing the relaxation model type is not achievable as long as the stress relaxation is plotted versus time on a linear scale. On this scale, All the models are identical to the exponential function, and they lay over each other. There is a simple method that can be followed to distinguish between linear and nonlinear behavior. By changing the axes scale to logarithmic, the models' representation is changed to improve the model type detection Figure 4.2.

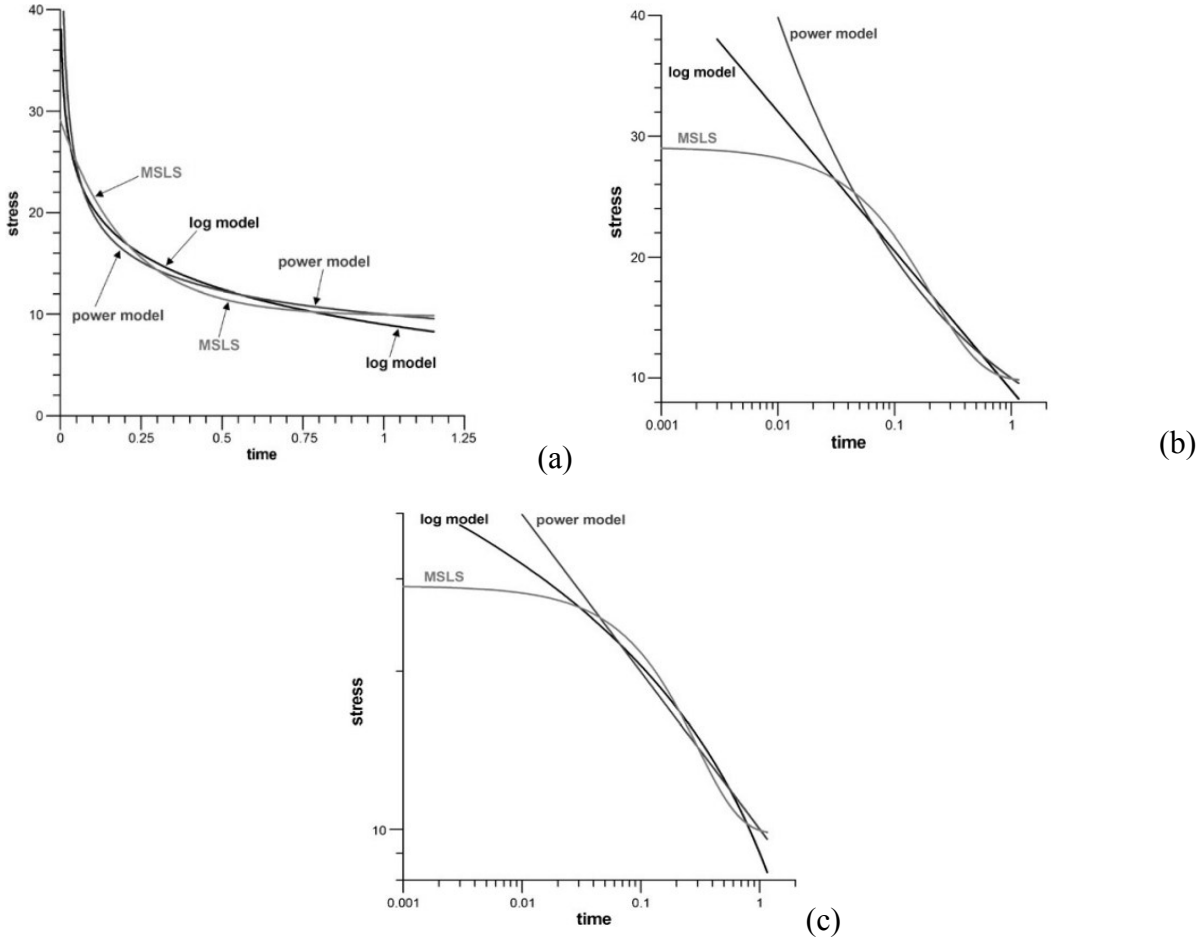

Figure 4. 2: Stress Relaxation of Linear, Power and Log models plotted in (a) linear (b) semi-logarithmic (c) Fully Logarithmic Scale [49]

4.3 Actual relaxation test

In practice, applying the unit step strain function with the unit impulse strain rate is not applicable because the crosshead displacement needs to be too high. Consequently, the actual loading condition divides into two sections. In the first section, the strain loading is considered as a ramp function with strain rate $\dot{\varepsilon}$. Then in the following section, the strain remains constant. The duration of the ramp section is known as the time delay. A higher strain rate results in a lower delay time equation; therefore, the obtained results get closer to the theory.

$$\varepsilon(t) = \begin{cases} \dot{\varepsilon} &) \le t \le \frac{\varepsilon_0}{\dot{\varepsilon}} \\ \varepsilon_0 & t \ge \frac{\varepsilon_0}{\dot{\varepsilon}} \end{cases} \qquad where: \quad \Delta t = \frac{\varepsilon_0}{\dot{\varepsilon}} \tag{4.14}$$

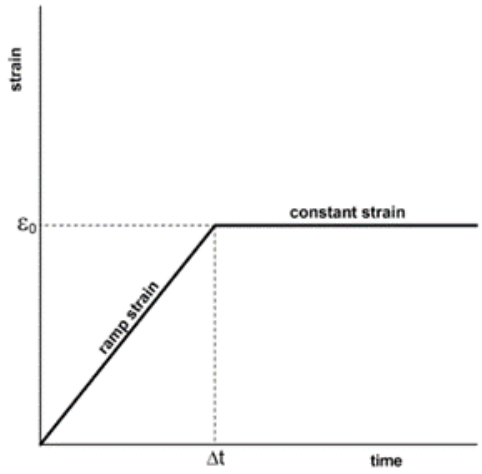

Figure 4. 3: Actual Test Condition [49]

The Laplace transform of the new strain loading condition is defined as follows

$$\mathcal{L}(\varepsilon) = \dot{\varepsilon}_0 \frac{1-e^{-s\Delta t}}{s^2 \Delta t} \quad [49] \tag{4.15}$$

Equation 4.15 was replaced in the constitutive functions of the proposed model. The mathematical method for the Laplace inverse is not available, so the transformed equations are calculated numerically to provide the relation of σ to ε_0 . Figures 4.2(c) and 4.4 illustrate the difference between the two strain loading conditions. By performing the test over a large time and removing data correspond to a short time, the effect of the initial ramp function could be eliminated.

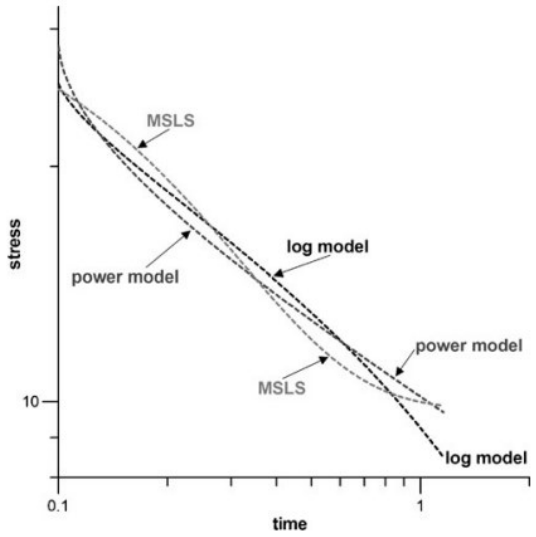

Figure 4. 4: Actual stress relaxation in logarithmic scale [49]

In chapter 5, the logarithmic scale of the stress relaxation test of our sample was presented. Also, Figure 4.4 shows the actual stress relaxation test for the nonlinear log model that has downward concavity similar to our experiment observation. So it can be concluded that the behavior of our sample is categorized into the nonlinear domain.

4.4 Proposed Nonlinear Model

The nonlinear viscoelastic approach for material characteristics that were developed earlier was proposed based on the theory of multiple molecular chains and validated for polymers; however, they are not suitable to describe the physics of more complex material like composites with a distinct morphology. Due to the limitation of the existing model, our motivation is to Figure out a new nonlinear viscoelastic model that can precisely cover a broad range of materials. The material with nonlinear behavior can vary from biomaterials to inorganics. This model not only has better accuracy in fitting with experiments observations but also can provide better prediction without implementing experiments. The model consists of much fewer parameters than the generalized Maxwell (Prony series) model. Also, all the expressed parameters in this model are meaningful in terms of physical characteristics and can provide a better demonstration of their effect. Moreover, the effect of fiber waviness in the elastic region and strain hardening or softening in plastic deformation can be illustrated through this approach.

In this approach, the material assumed as a micro-network consists of an elastic network with viscous media Figure 4.5. The elastic element represents the fiber component, and the elastic modulus of the resin and the viscous media denotes the resin. Obviously, viscosity is temperature and rate-dependent. Several linear viscous model can be considered for resin; however, to take into account more complexity in our study, we model this behavior as power-law [50].

$$\eta(t) = \mu\left(\frac{t}{\tau}\right)^{\alpha} \tag{4.16}$$

Where α is a model parameter, μ is viscosity parameter (MPa.s), and τ is retardation time that is a function of temperature. In other words, when the tested temperature is the same as the reference temperature $\tau = 1$ and when it is not equal to the reference temperature, the value of this parameter should be calculated through the time-temperature superposition principle (TTS) that

was developed for viscoelastic materials. The shape of the curve of the relaxation modulus of linear viscoelastic material does not change as the temperature increases and just shifts through time. As a result, this concept indicates that the mechanical properties of viscoelastic material, such as relaxation in high temperature, are equivalent to the same property at reference temperature for a longer time. So this method can perfectly predict the behavior of the material at a given temperature by using shift operation. The shift operator is calculated empirically. The most established models are Williams-Landel-Ferry (WLF) and Arrhenius. WLF model proposed by the following relation [51]:

$$\log a_T = -\frac{C_1(T-T_0)}{C_2+(T-T_0)} \tag{4.17}$$

Where C_1 and C_2 are constants that be defined according to the material and reference temperature. This model is applicable only in the range of [T_g , T_g+100$^\circ C$]. Arrhenius law is defined as below [52]:

$$\log a_T = -\frac{E_a}{2.303R}\left(\frac{1}{T}-\frac{1}{T_0}\right) \tag{4.18}$$

Where E_a is the activation energy, R is the universal gas constant, and T_0 is a reference temperature in kelvin. This principle is applicable for temperatures lower than glass transition (T_g). As it was mentioned earlier, the available shift factor operations are not tangible in predicting nonlinear viscoelastic behavior in higher temperatures. In section, this concept was elaborated and compared to experimental observation. As it was mentioned before, in viscoelastic material, we have energy dissipation, so this phenomenon can be explained by the internal friction between two components. Actually, viscosity can be known as friction in fluid; therefore, it could be concluded that μ can also be considered as a friction coefficient between elastic network and viscous media in the model. α parameter can be dedicated as a module for defining the sensitivity of the model to time and temperature. It means that a higher alpha value will result in a higher variation of modulus. This claim can be proved through molecular theories.

This model can also be illustrated by the configuration of springs and dashpot. Same as linear models, the layout of the model was selected as Maxwell model with nonlinear dashpot model. The strain was applied to the system as a Heaviside function, then the relation of the stress and

strain was derived. At last, after solving the derived differential equation, the relation of stress with strain as well as relaxation modulus can be concluded.

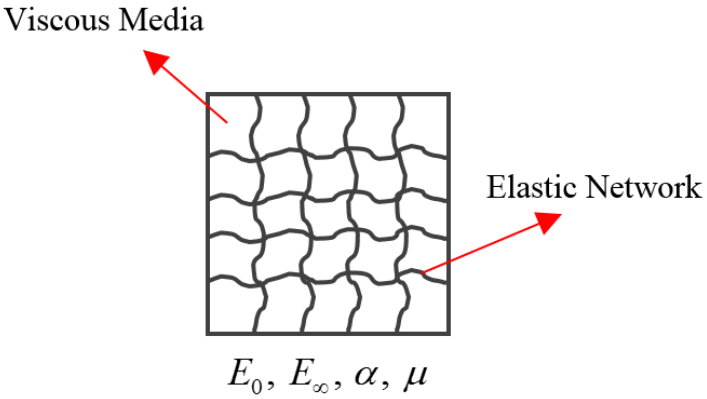

Figure 4. 5: Micro Structure of Proposed Nonlinear Model

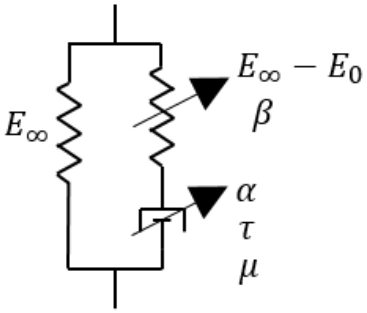

$$\varepsilon_0 H(t) = \varepsilon_1 + \varepsilon_2$$
$$\sigma(t) = E_\infty \varepsilon_0 H(t) + (E_\infty - E_0)\varepsilon_1$$
$$(E_\infty - E_0)\varepsilon_1 = \eta(t)\dot{\quad}$$
$$\varepsilon_1 = \varepsilon_0 H(t) e^{-\frac{\tau(E_\infty - E_0)}{(1-\alpha)\mu}\left(\frac{t}{\tau}\right)^{1-\alpha}} \tag{4.19}$$
$$E(t) = \frac{\sigma(t)}{\varepsilon_0 H(t)} = E_\infty + (E_\infty - E_0) e^{-\frac{\tau(E_\infty - E_0)}{(1-\alpha)\mu}\left(\frac{t}{\tau}\right)^{1-\alpha}}$$

Where ε_1 and ε_2 are the strain of spring and dashpot, respectively, $E_\infty - E_0$ is the difference between the instant and infinite modulus. The result shows the exponential decay so that at the beginning of the test, the instant modulus is E_0 , and as time goes on, the final modulus converges to E_∞ in infinite time.

According to the stress-strain curve obtained from the tensile test on the prepreg, the plot can be classified into two different regions due to the presence of fiber waviness and corresponding to the deformation rate—nonlinear region proceeding to linear region Figure. For example, with the rate of 2mm/s, the nonlinear section rests in the strain range of less than 0.25%. Regardless of the deformation rate, the slope of the linear region denotes the elastic modulus in the prepreg in the fiber direction, shown in Figure 4.6. This value is in good agreement with the reported value E_1 in [53]. That is also equivalent to relaxation modulus at t=0.

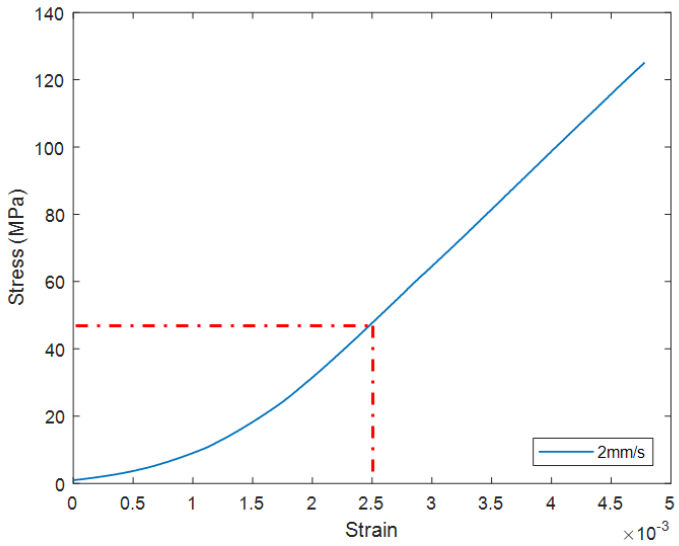

Figure 4. 6: Average Experimental Results of the Tensile Behavior of Uncured Prepreg

In our relaxation test, the applied strain ε_0 is 0.36%, which is more than the transient strain point. So, it can be concluded that the proposed model can perfectly predict the linear region for strain value greater than 0.25% assuming the spring as a linear element. However, for the nonlinear region, the spring element must be considered as a function of strain. The relation of stress versus strain is nonlinear, so one way to eliminate this nonlinearity is to break down the region into several linear lines. Figure 4.7 shows six linear lines with their slope creating the nonlinear curve. By modifying spring elements in equation 4.16 in table 4.1, the relaxation modulus will be defined for each strain range individually. For this purpose, $E_0(t)$ in the formulations should be replaced by $E^*(\varepsilon)$. It can be concluded that the relaxation modulus is not only a function of time and temperature but also a function of strain.

Strain Range (ε)	Section Modulus (E^* (MPa))
0-0.0004	4981.8
0.0004-0.0008	9116.2
0.0008-0.0012	14396
0.0012-0.0016	21264
0.0016-0.002	27789
0.002-0.0024	32480

Table 4. 1: the value of section modulus correspond to different strain range in the nonlinear region

$$E(t,\varepsilon)=\frac{\sigma(t)}{\varepsilon_0 H(t)}=E_\infty+(E_\infty-E^*(\varepsilon))e^{-\frac{\tau(E_\infty-E^*(\varepsilon))}{(1-\alpha)\mu}\left(\frac{t}{\tau}\right)^{1-\alpha}} \tag{4.20}$$

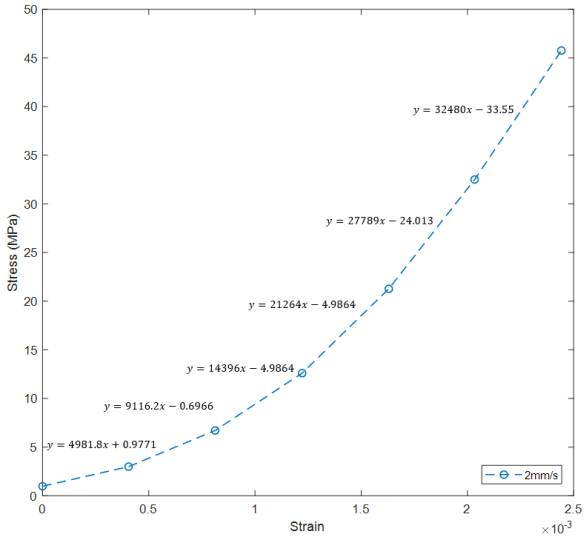

Figure 4. 7: Linear trend lines Fitted on Non-Linear Region

Uncured prepregs are not undergone large strain deformation in the manufacturing and forming process, so they rarely enter to plastic deformation before failure. But just in case if the applied strain is quite large, the plastic deformation can be characterized as strain hardening or softening. To consider the hardening and softening properties of the model, the spring is considered a nonlinear hardening or softening equation. The relation between force and the displacement was shown in Figure 4.8 [54].

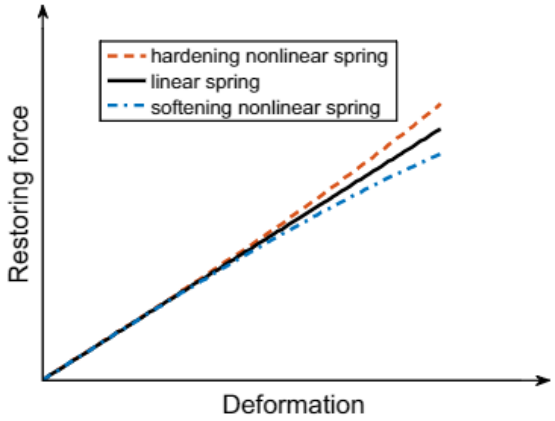

Figure 4. 8: Force vs. Deformation for nonlinear spring [54]

And the constitutive law is

$$F = kx + \beta x^3 \qquad \text{(Nonlinear Spring)} \qquad (4.21)$$

Where β is a coefficient expressing the nonlinear strain behavior. If $\beta > 0$ the spring is hardening, when $\beta < 0$, it is softening and for $\beta = 0$ it acts like linear spring. In our terminology, F corresponds to σ, the displacement (x) is replaced by ε_1 and k replaced by to $E_\infty - E_0$ then by substituting into the constitutive equations the relaxation modulus will.

$$E(t) = \frac{\sigma(t)}{\varepsilon_0 H(t)} = E_\infty + (1+\varepsilon)^\beta (E_\infty - E_0) e^{-\frac{\tau(E_\infty - E_0)}{(1-\alpha)\mu}\left(\frac{t}{\tau}\right)^{1-\alpha}} \tag{4.22}$$

The proposed model could be a better choice for experimental data fitting rather than PS model. First, it consists of fewer parameters and provides less complexity for interpreting the material physical behavior. Second, the large number of parameters can tend to instability and cause data overfitting. Last but not least, the large spring-dashpot configuration of PS cannot model the complex materials properly with multiphase components. PS can only be fitted precisely only within the time range of available data, and out of the data range, the parameters are likely to converge to false values. Nevertheless, data fitting using PS is still acceptable because of its high accuracy in the data range. More importantly, it is a robust tool for implementing finite element analysis due to providing a closed-form solution for time integration.

4.5 Model parameter acquisition

4.5.1 Optimization method

The proposed model is highly nonlinear, so the fitting process demands an advanced optimization algorithm to provide the best result. In this study trust-region method (TRM) was utilized. This method is known as one of the most important numerical optimization techniques in solving nonlinear programming. In the first step of this method, a specific region (usually as a spherical with a known radius) was defined around the current solution Figure 4.9 Then, TRM approximates the objective function using a model function. If any proper estimation is found within the trust region, the region will expand.

On the other hand, if the approximation is poor, the region is contracted. A threshold is defined to represent the expansion and contraction of the area. At last, the model function is trusted only in the region where the satisfactory approximation is given. The algorithm was described below

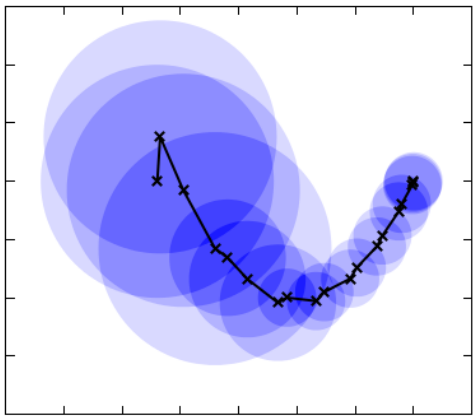

Figure 4. 9: Iteration procedure of trust-region Optimization [55]

The starting point is set to x_0

The iteration number $k = 1$

for $k = 1, 2, \ldots$

Obtain the improving step by solving the trust-region subproblem

Evaluate ρ_k

if $\rho_k < \eta_2$

$\Delta_{k+1} = t_1 \Delta_k$

else

if $\rho_k > \eta_3$ **and** $p_k = \|\Delta_k\|$ (good approximation)

$\Delta_{k+1} = \min(t_2 \Delta_k, \Delta_M)$

else

$\Delta_{k+1} = \Delta_k$

if $\rho_k > \eta_1$

$x_{k+1} = x_k + p_k$

else

$x_{k+1} = x_k$ (The model is not a good approximation, so the solver requires a smaller region)

end

Trust Region Algorithm

Where Δ_k is an area radius, ρ_k is model's validity function, η_1, η_2, η_3 are the threshold value for evaluation the goodness, and t_1, t_2 are adjusting coefficient to modify the region radius in each iteration.

4.5.2 The goodness of the fit

To measure the perfectness of our fit and assess the quality of model predictor, the statistical manipulation was implemented. The mean square error (MSE) [56] was used to measure the average squared difference between the estimated and actual values. In other words, it is derived from the square of Euclidean distance. The MSE is always positive, and the lower the value results in higher accuracy.

$$MSE = \frac{\left\| x - x_{ref} \right\|^2}{N} \tag{4.23}$$

Where N is the number of samples, and the second norm of a deference vector is shown in the nominator. Actually, there is no acceptable limit for MSE, so the lower MSE, the higher the accuracy.

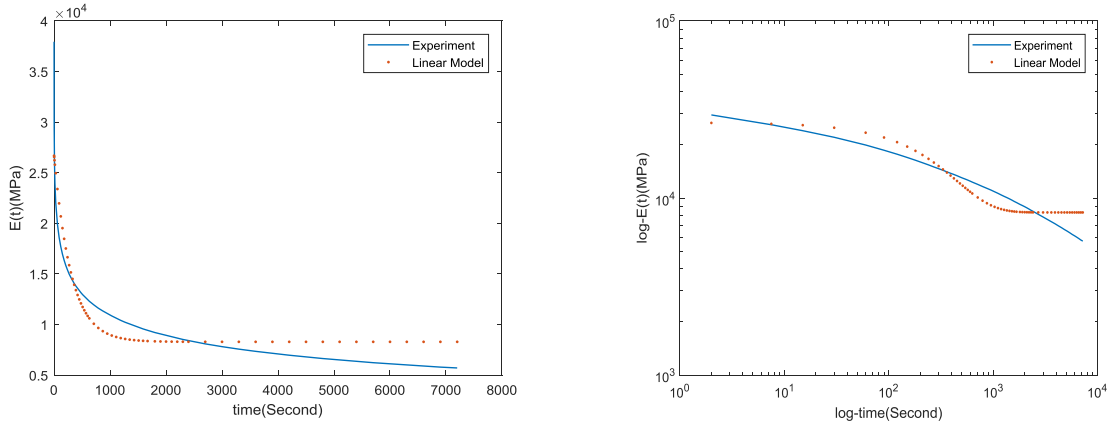

Figure 4. 10: Model fits of relaxation modulus using Maxwell model

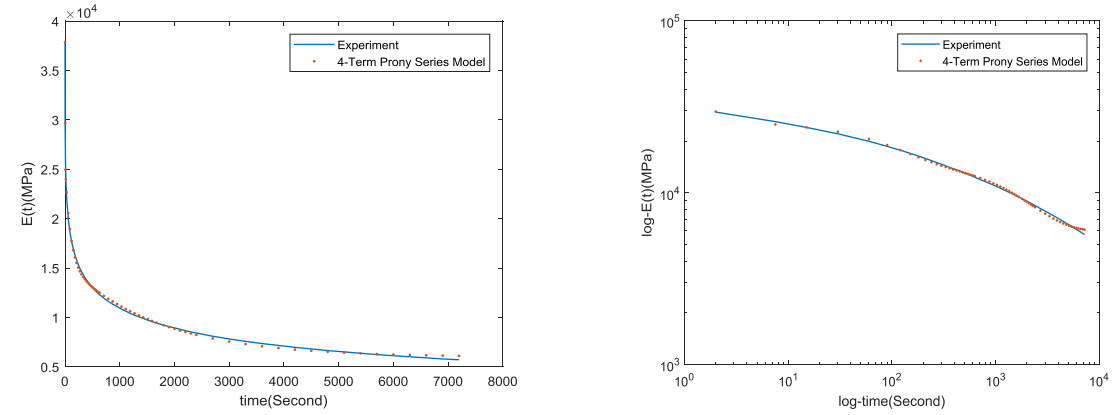

Figure 4. 11: Model fits of relaxation modulus using 4-term Prony model

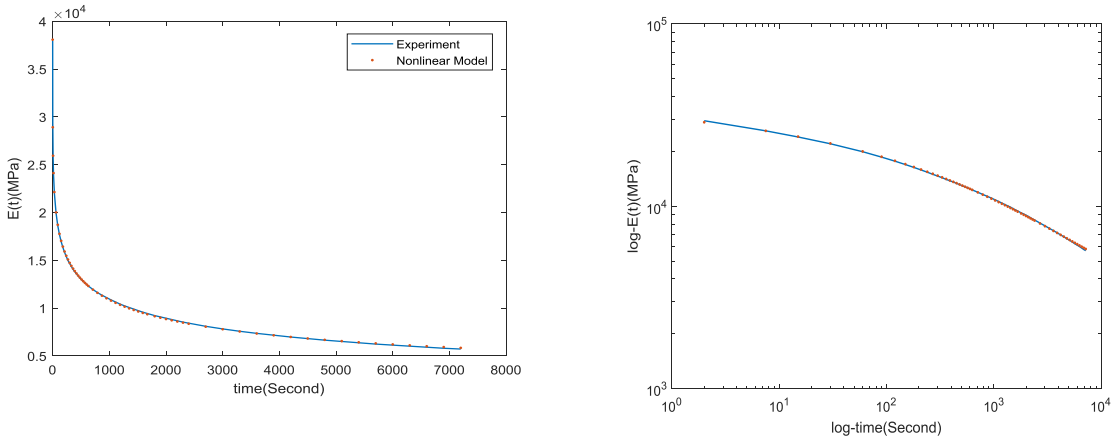

Figure 4. 12: Model fits of relaxation modulus using proposed nonlinear model

E_∞	E_0	τ_R	MSE ($\times 10^5$)
8294.73	26681.8	304.35	48.87

Table 4. 2: Maxwell Model Parameters

E_∞	E_0	α	μ	τ_R	MSE ($\times 10^5$)
2740.07	38075.65	0.74	549616.5	1	0.10136

Table 4. 3: Nonlinear Proposed Model Parameters

R_1	R_2	R_3	R_4	η_1	η_2	η_3	η_4	MSE ($\times 10^5$)
5976.30	9473.23	12397.87	10041.64	∞	1673.96	1.93	97.84	0.7

Table 4. 4: 4-Term Prony Model Parameters

In table 4.2-4.4 The models' parameters were defined through the optimization method. Based on the MSE metric criterion. It can be observed that not only the nonlinear model is the most accurate fit to the experimental observation, but also it can provide the best prediction outside the experimental range.

4.6 Bending analysis

There are several works that have been accomplished on theoretical modeling of the bending behavior of dry textiles, such as the energy approach [57], phenomenological model [58], and linear elastic model [59]. These proposed models might be valid for dry fibers; however, for composite materials, especially uncured composites, because of the presence of the viscous matrix,

fibers are much less deformable compared to matrix. Therefore fiber and matrix cannot behave in elastic but in a viscoelastic manner. In this section, the Bending analysis was implemented for linear and nonlinear viscoelastic models, which was proposed for uncured prepreg. After comparing the approaches, according to the experimental observation, the decision was made which model can better depict the bending behavior of the material. For the linear approach, the integro-differential equation was obtained, and for the nonlinear method, the integral technique was conducted.

Based on testing observations, the uncured prepreg can easily be deformed, and the bending mechanism can cause large deflections/slopes while strains remain small. In our study, the prepreg was assumed as an integrated uniform cantilever viscoelastic beam at the macro scale. Euler-Bernoulli beam theory was followed in deriving a mathematical model. Since the beam was bent under its own weight, the loading condition can be considered uniformly distributed.

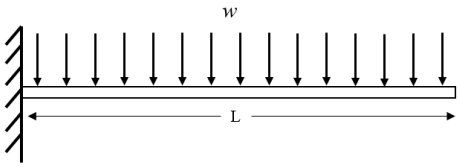

Figure 4. 13: Cantilever viscoelastic beam subjected to uniformly distributed load

4.6.1 Linear Viscoelastic bending model

There are some assumptions that need to be considered during the analysis. First of all, the Maxwell model is chosen for the viscoelastic model. Secondly, axial extension and shear deformation of the beam are neglected.

Stress-strain relation in linear viscoelastic material is represented as relations below. The instantaneous creep and relaxation terms are ignored.

$$\sigma(t) = \int_0^t E(t-\tau)\frac{d\varepsilon(\tau)}{d\tau}d\tau \tag{4.24}$$

$$\varepsilon(t) = \int_0^t J(t-\tau)\frac{d\sigma(\tau)}{d\tau}d\tau \tag{4.25}$$

Where E, J denote relaxation modulus and creep compliance, respectively, and τ known as the integral variable of time. The relationship between relaxation modulus and creep compliance in time and Laplace domain are shown below

$$\int_0^t E(t-\tau)\frac{dJ(\tau)}{d\tau}d\tau = 1 \qquad AND \qquad \hat{E}(s)\hat{J}(s) = \frac{1}{s^2} \tag{4.26}$$

Hence by knowing the formulation of relaxation modulus provided that its Laplace transformation is invertible, the constitutive function of creep compliance can be achieved.

In accordance with the first assumption, the Maxwell model is selected as our linear model. Where equivalently, R_2 and R_1 replaced by $E_0 - E_\infty$ and E_∞ sequentially and τ_R denotes relaxation time equivalents to η / R_2

$$E(t) = E_\infty + (E_0 - E_\infty)e^{-\frac{t}{\tau_R}} \tag{4.27}$$

By substituting equation 4.27 in equation 4.26, by implementing the Laplace inverse, creep compliance will be derived for the Maxwell model.

$$J(t) = J_\infty + (J_0 - J_\infty)e^{-\frac{t}{\tau_c}} \tag{4.28}$$

Where J_0, J_∞, E_0 *and* E_∞ are related through $J_0 = 1/E_0$ *and* $J_\infty = 1/E_\infty$. Also τ_c represents creep times characteristic is related to τ_R by $\tau_R = (E_\infty / E_0)\tau_c$.

The mathematical representation for bending analysis is conducted by considering the geometrical compatibility, equilibrium of forces and moments, and linear viscoelastic law.

By extracting infinitesimal elements from the beam, the following geometrical relations are obtained.

$$\frac{\partial x(s,t)}{\partial s} = \cos(\theta(s,t)) \tag{4.29}$$

$$\frac{\partial y(s,t)}{\partial s} = \sin(\theta(s,t)) \tag{4.30}$$

$$\frac{\partial \theta(s,t)}{\partial s} = k(s,t) \tag{4.31}$$

x(s,t), y(s,t) represents the Cartesian coordinates of each point on the deflected beam. *s* is the arc length measured from the fixed end, *t* is the current time, $\theta(s,t)$ indicated the slope and, *k(s,t)* denotes beam curvature or deflection.

The analysis is considered in a quasi-static equilibrium state at each time. So the shear force relation can be derived under distributed force.

$$V(s,t) = \frac{dM(s,t)}{ds} = -ws\cos(\theta(s,t)) \tag{4.32}$$

Where w signifies uniformly distributed force per length.

The constitutive law for stress-strain of the linear viscoelastic material, when subjected to uniaxial load, can be defined in terms of relaxation and creep functions.

$$\sigma(s,t) = E(0)\varepsilon(s,t) + \int_0^t \varepsilon(s,t)\frac{\partial E(t-\tau)}{\partial(t-\tau)}d\tau \qquad \text{(Relaxation Function)} \tag{4.33}$$

$$\varepsilon(s,t) = J(0)\sigma(s,t) + \int_0^t \sigma(s,t)\frac{\partial J(t-\tau)}{\partial(t-\tau)}d\tau \qquad \text{(Creep Function)} \tag{4.34}$$

Since the element is static equilibrium, the bending moment equation of sectioned area is found below

$$M(s,t) = \int \sigma(s,t)ydA \tag{4.35}$$

Where y is the distance from the neutral axis, as mentioned before, the beam is assumed as Euler Bernoulli. So the relation of slope and bending moment are provided through the theory.

$$I\frac{\partial\theta(s,t)}{\partial s} = \int_0^t J(t-\tau)\frac{\partial M(s,\tau)}{\partial\tau}d\tau \tag{4.36}$$

Where I is the moment of inertia of the cross-section.

By differentiating equation 4.36 with respect to s, equation 4.37 is issued.

$$I\frac{\partial^2\theta(s,t)}{\partial s^2} = -ws\int_0^t J(t-\tau)\frac{\partial}{\partial\tau}\cos(\theta(s,\tau))d\tau \tag{4.37}$$

Assuming that there is no load applied prior to the instant time t=0, the integration of the right-hand side of equation 4.37 is given as follows.

$$I\frac{\partial^2\theta(s,t)}{\partial s^2} = -ws\times[J(0)\cos(\theta(s,\tau)) - \int_0^t J'(t-\tau)\cos(\theta(s,\tau))d\tau] \tag{4.38}$$

Combining equation 4.38, 29-31, the governing equations for bending behavior is obtained in the form of nonlinear partial Integro-Differential (PID). These equations are applicable for either linear or nonlinear viscoelastic models provided that the Creep function *J* is known. However, according to equation 4.26, Obtaining *J* function from *E* function is not possible for the nonlinear model. So in order to overcome this problem, creep constitutive equations should be developed individually.

To provide general solution for developed equations, the parameters are changed to non-dimensional form by using the following relations.

$$\begin{aligned}
&\frac{\partial \bar{x}(\bar{s},\bar{t})}{\partial \bar{s}} = \cos(\bar{\theta}(\bar{s},\bar{t})) \\
&\frac{\partial \bar{y}(\bar{s},\bar{t})}{\partial \bar{s}} = \sin(\bar{\theta}(\bar{s},\bar{t})) \\
&\frac{\partial \bar{\theta}(\bar{s},\bar{t})}{\partial \bar{s}} = \bar{k}(\bar{s},\bar{t}) \\
&\frac{\partial \bar{k}(\bar{s},\bar{t})}{\partial \bar{s}} = -\bar{w}\bar{s}\left[\cos(\bar{\theta}(\bar{s},\bar{t})) + (\alpha-1)\int_0^{\bar{t}} \bar{w}\cos(\bar{\theta}(\bar{s},\bar{t}))e^{-(\bar{t}-\bar{\tau})\alpha} d\bar{\tau}\right]
\end{aligned} \tag{4.39}$$

Where $\bar{s} = s/L\,(0<s<1)$, $\bar{x} = x/L$, $\bar{y} = y/L$, $\bar{t} = t/\tau_R$, $\bar{k} = kL$, $\bar{w} = wJ_0L^3/I$ and $\alpha = G_\infty / G_0$ or J_0 / J_∞ (4.40)

As previously stated, the prepreg was assumed as a cantilever beam that was constrained at one end. So the boundary condition that corresponds to this problem was defined as follows.

$$x(0,t) = y(0,t) = \theta(0,t) = k(L,t) = 0 \tag{4.41}$$

x,y displacement, and rotation (θ) at the fixed end are zero as well as deflection at the free end for all time.

For the purpose of solving the system of four non-linear partial integro-differential (PID) equations in terms of independent variables of *t* and *s*, fourth-order Runge-kutta (RK4) method was used. This method provides a solution only for the problems with the initial condition. However, this system is a boundary condition problem. So to make this method applicable to our problem, the shooting method was accompanied along with RK. The shooting method is a tool to convert the boundary condition problem into an initial condition problem. The RK coupled with the shooting method works in a manner of guessing one initial condition by trial and error, then the system of differential equations was solved though RK corresponds to the guessed value. The estimation of

the initial value was continued till the sign of the boundary value changed. Obviously, it was concluded that the corresponding root must be located between the previous guess and the new one, so by means of the Newton-Raphson (Bisection) method, the root was defined. This task was repeated iteratively until the boundary condition reached the desired value. In order to reduce the computation time, the previously obtained value for the curvature can be used for the initial guess of the curvature for the next time step. For instance, $\bar{k}(0,\bar{t}+1)$ can be selected from the range of $(0.8\bar{k}(0,\bar{t}),\ 1.2\bar{k}(0,\bar{t}))$

The utilization of the RK method for a system of equations 4.39 provides as follows:

$$\bar{\theta}(m+1,i)=\bar{\theta}(m,i)+\frac{\Delta s}{6}(k_{\theta 1}+2k_{\theta 2}+2k_{\theta 3}+k_{\theta 4}) \tag{4.42}$$

$$\bar{k}(m+1,i)=\bar{k}(m,i)+\frac{\Delta s}{6}(k_{k1}+2k_{k2}+2k_{k3}+k_{k4}) \tag{4.43}$$

Since k and θ are a function of two independent variables s and t, therefore, two sets of recurrence relationships are required.

$$\begin{aligned}
k_{\theta 1} &= f_\theta(\bar{k}(m,i)) & k_{k1} &= f_k(\bar{\theta}(m,i)) \\
k_{\theta 2} &= f_\theta(\bar{k}(m,i)+\Delta s\frac{k_{k1}}{2}) & k_{k2} &= f_k(\bar{\theta}(m,i)+\Delta s\frac{k_{\theta 1}}{2}) \\
k_{\theta 3} &= f_\theta(\bar{k}(m,i)+\Delta s\frac{k_{k2}}{2}) & k_{k3} &= f_k(\bar{\theta}(m,i)+\Delta s\frac{k_{\theta 2}}{2}) \\
k_{\theta 4} &= f_\theta(\bar{k}(m,i)+\Delta s k_{k3}) & k_{k4} &= f_k(\bar{\theta}(m,i)+\Delta s k_{\theta 3})
\end{aligned} \tag{4.44}$$

Considering $\lambda\in\{\theta,k\}$, $k_{\lambda 1}$ is the slope at the beginning of the interval, $k_{\lambda 2}$ is the slope at the midpoint of the interval, using λ and $k_{\lambda 1}$, $k_{\lambda 3}$ is the slope at the midpoint, using λ and $k_{\lambda 2}$, last but not least, $k_{\lambda 4}$ is the slope at the endpoint of the interval.

The incremental governing functions developed from the RK4 method are obtained as below

$$f_\theta(\bar{k}(m,i))=\bar{k}(m,i) \tag{4.45}$$

$$\begin{aligned}
f_k(\bar{\theta}(m,i)) = -\bar{w}\times m\times ds\{&\cos(\bar{\theta}(m,i)) \\
&-(\alpha-1)\frac{\Delta t}{2}\left[\sum_{j=0}^{i-1}\cos(\bar{\theta}(m,j))e^{-\alpha(i-j)\Delta t}+\cos(\bar{\theta}(m,j+1))e^{-\alpha(i-(j+1))\Delta t}\right]\}
\end{aligned} \tag{4.46}$$

This method can incrementally solve the problem from the initial time up to the required time. Where Δs and Δt are spatial and time increments and $m = s / \Delta s$, $i = t / \Delta t$. It can be seen that the relations between constitutive components of equations 4.42-46 are recursive, so the solution of the previous time step is required to derive the solution for the current step. These statements can truly prove the time dependency of the viscous material in the bending mechanism.

In order to apply this approach to our case study, the testing parameters must be nondimensionalized. From table 3.2, using sets of equations 4-40 $\bar{w} = 2.064$, $\alpha = 0.31$ were identified. $\bar{s} = 1$ and $\bar{t} = 60$ discretized into *m*=11 and *i*=60 with increment steps of $\Delta s = 0.1$ and $\Delta t = 2$ respectively. Finally, after applying parameters into 4.42-46, the value of θ and k in the time and space domain can be derived using the RK4 method. Also, through solving equations 4.47,4.48. x and y coordinates can be calculated. Simpson's one-third rule was used for integration. This numerical method needs the odd number of integration points; that's why eleven discrete points were selected for the space domain.

$$\bar{x}(\bar{s},\bar{t}) = \int_0^{\bar{s}} \cos(\bar{\theta}(\eta,\bar{t}))d\eta \tag{4.47}$$

$$\bar{y}(\bar{s},\bar{t}) = \int_0^{\bar{s}} \sin(\bar{\theta}(\eta,\bar{t}))d\eta \tag{4.48}$$

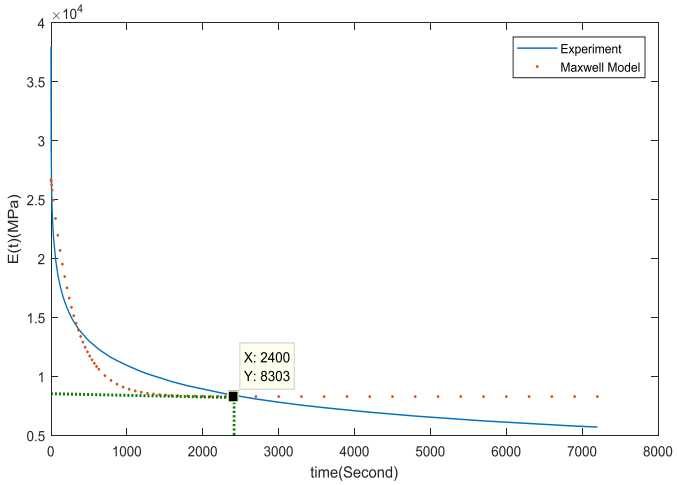

Figure 4. 14: linear Maxwell relaxation modulus model versus experiment results

Figure 4.14 shows that prior to 2400s(45min), the Maxwell model can fit well on experimental data. After this time, the Maxwell model converges to a certain asymptote while the experiment continues to decline; thus, two graphs begin to diverge. So it can be concluded that the nonlinear model can be replaced by a linear model for a small time period. Moreover, Figure 4.15 illustrates

the non-dimensional vertical tip displacement $(\bar{y} \ \ at \ \ \bar{s}=1)$ with respect to non-dimensional time $(\bar{t})$.This indicates that the two graphs coincide approximately for $\bar{t}$ less than 8(40.52min). Two margins of time derived from experiments and the bending model are in good agreement. Consequently, the proposed bending model can also prove this claim and can function well for a small-time period.

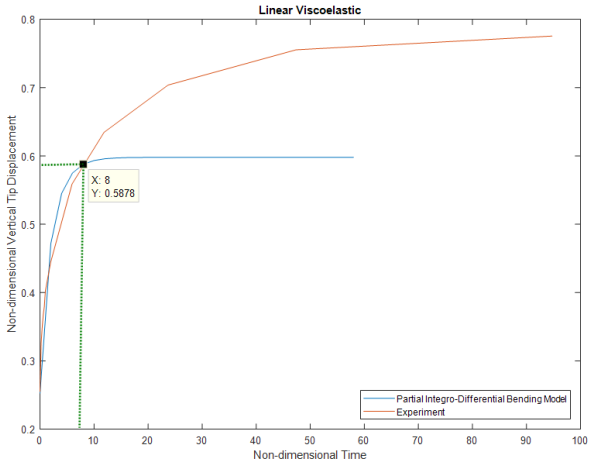

Figure 4. 15: non-dimensional vertical tip displacement solved through PID model versus Experiment

In addition, Figure 4.16 shows the relation of non-dimensional fixed-end curvature $(\bar{k} \ \ at \ \ \bar{s}=0)$ as a function of time (t). Based on the previous claim that the Partial Integro-Differential model developed for the linear viscoelastic model can adequately depict the nonlinear viscoelastic behavior of sample for a time period less than 45min, it can be observed that at $t \approx 0,5,30\,\text{min}$ the non-dimensional parameter of curvature $\bar{k}$ derived from the experiment and the proposed model are in a good agreement.

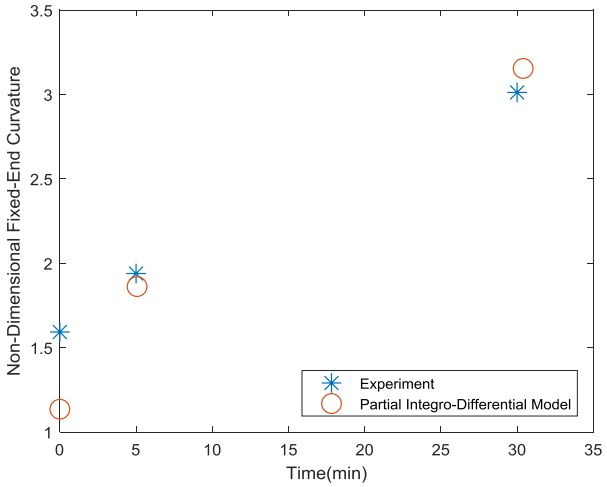

Figure 4. 16: Non-dimensional fixed end curvature of experiment and PID model at 0, 5, and 30min time instant

4.6.2 Linear Viscoelastic bending model

This section addresses a method known as the integral approach to predict the bending behavior of nonlinear viscoelastic beams. In this approach, the viscoelastic beam was considered as an elastic beam in each time step with relaxation modules corresponding to that time. At each time frame, theta and M are considered time-invariant, and they are the only function of distance along the beam, while E^t is different at each time. Equation 4.49 represents The relation of bending moment and beam deformation based on Euler-Bernoulli's theory at the individual timeframe.

$$\frac{d\theta(s)}{ds} = \frac{M(s)}{E_t I} \tag{4.49}$$

In the case of a large deflection equation 4.49 changes to 4.50

$$\frac{\frac{d^2y}{dx^2}}{\left[1+\left(\frac{dy}{dx}\right)^2\right]^{3/2}} = \frac{M(x)}{E_t I} \tag{4.50}$$

The left side of the equation 4.50 equals deflection, and *x, y* represents the horizontal and vertical coordinates of the beam's point. By transforming the dy/dx variable into z and substituting it into equation 4.50, the relation can be rewritten.

$$\frac{dz}{(1+z^2)^{3/2}} = \frac{M(x)}{E_t I}dx \tag{4.51}$$

Equation 4.51 is integrated as a result variable χ as a function of x is introduced.

$$\frac{z}{\sqrt{1+z^2}} = \int_0^x \frac{M(x)}{E_t I}dx = \chi(x) \tag{4.52}$$

From equation 4.52 where $z=dy/dx$, the new governing equation of bending for cantilever beam can be depicted as follow.

$$\frac{dy}{dx} = \frac{\chi(x)}{\sqrt{1-\chi^2(s)}} \tag{4.53}$$

The loading condition is considered as uniformly distributed load (w), applied on the entire beam downward aligned with the y-axis. Moreover, because of the low bending stiffness of uncured prepreg, the sample is undergone large deformation. Hence, the relation of the moment as a function location of the beam's point for large deflection is written as follows:

$$M(s) = \int_s^L w[x(\eta) - x(s)]d\eta \tag{4.54}$$

An analytical approach is not feasible to solve equation 4.54. Therefore, M and χ should be solved numerically. For this purpose, the beam is segmented into N elements by $N+1$ nodes, $s_0, s_1, ..., s_N$ are the segments curve length where s_N assigned as the whole beam length equals L. The corresponding coordinates are named $(x_0, y_0), ..., (x_N, y_N)$. The discretized format of equations 4.52 and 4.54 are provided as follows

$$M_i = \sum_{j=i+1}^{N} w(s_j - s_{j-1})\left(\frac{x_{j-1}+x_j}{2} - x_j\right) \qquad where \;\; i = 0, ..., N-1 \; and \; M_N = 0 \tag{4.55}$$

$$\chi_i = \chi_{i-1} + \left(\frac{M_{i-1}+M_i}{2E_t I}\right)(x_i - x_{i-1}) \qquad where \; \chi_0 = 0 \tag{4.56}$$

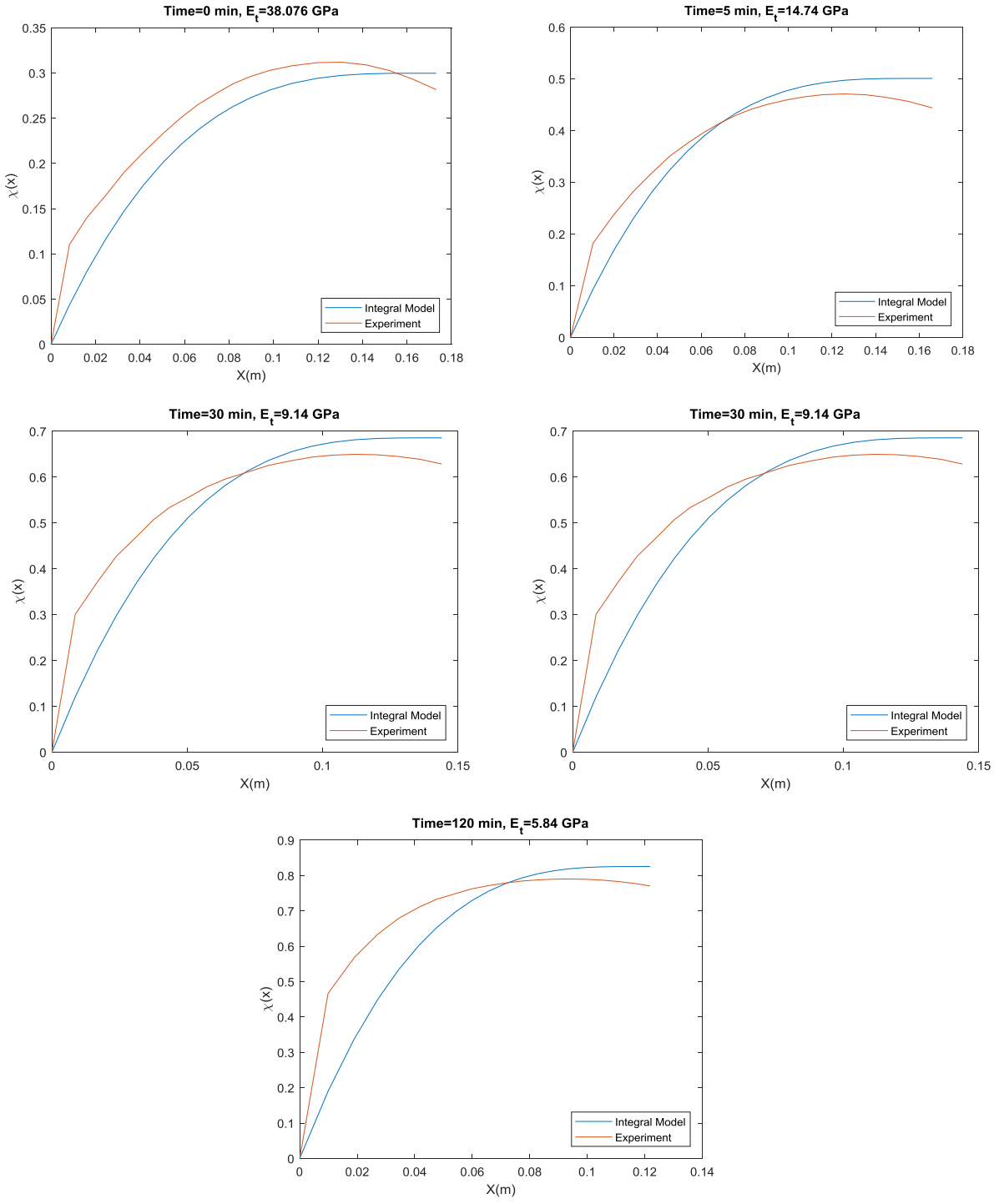

Figure 4. 17: Demonstration of χ parameter as a function of X derived from Integral model and Experiment

According to the proposed method, M and χ can be calculated at every spatial node named i for a specific time step as the value of E_t remains constant as long as the time step is not changed. As time moves forward, all these calculations should be repeated with the new E_t value. The amount of E_t is derived from the proposed nonlinear viscoelastic model. The mathematical relations of

both sides of equation 4.52 must be equivalent, so in order to evaluate the feasibility of this approach, we can use χ parameter as an assessment criterion. χ parameter can be calculated through either side of equation 4.52 .The left-hand side is a function of z, known as the slope of the bending curve, so by knowing the coordinates of the curve, the value χ can be obtained experimentally. The alternative means to obtain χ , is solving the integral relationship that is on the right-hand side of equation 4.52. The numerical approach to solve this integral is mentioned in the previous section. Figure 4.17 shows the χ parameter as a function of x derived from the left (experiment) and right (integral model) sides. It can be seen that the integral model and experiment results are in good agreement. So it can be concluded that the assumption that the viscoelastic beam can be considered an elastic beam at each instant with different E_t is acceptable.

5 Finite element analysis

Forming simulation is a great tool to provide an initial estimation of forming in determining desirable parameters of the process. The finite element method (FEM) could be suitable for this purpose and can significantly reduce the costs of the design process causing by the trial and error technique. In Figure 5.1, the deformation of dry textile reinforcement analogous to composite prepreg was simulated. The effect of different deformation mechanisms and their coupling was illustrated. It can be concluded that consideration of all mechanisms can result in better wrinkle prediction.

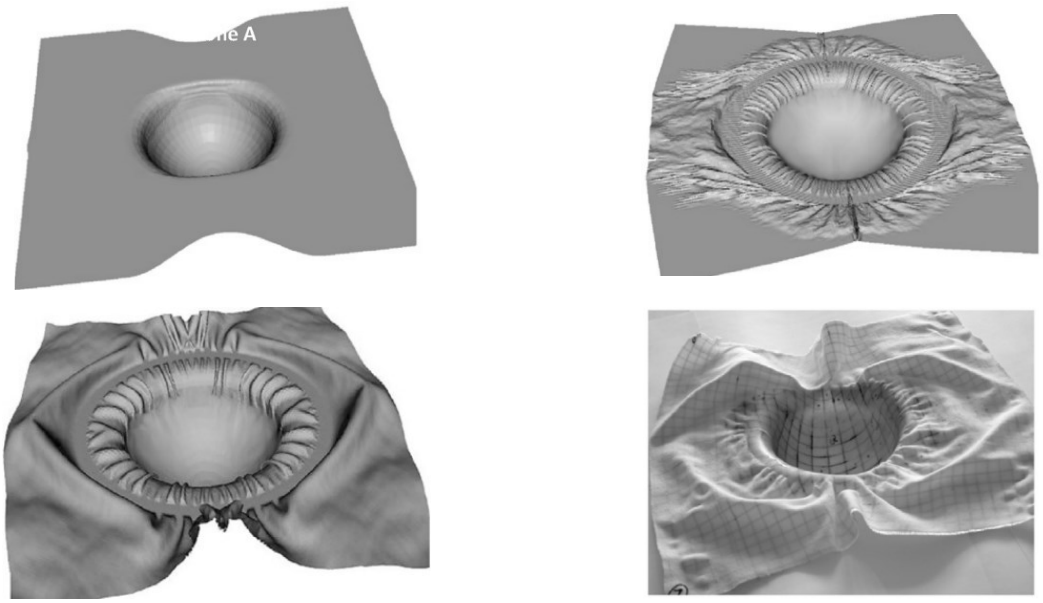

Figure 5. 1: Effect of forming parameters on Dry textile reinforcement forming simulation (a) tensile only (b)tensile and in-plane shear (c) tensile, in-plane shear, and bending (d) Experimental Forming [16]

Some commercial composite forming platforms are available such as Pam-Form™ [60] and AniForm™ [61], which are based on explicit and implicit approaches, respectively. As it was mentioned earlier, bending behavior has a significant role in predicting the wrinkle during forming. The FEM model must be customized in order to consider the effect of bending behavior. For this purpose, since the bending rigidity is much lower than fiber stiffness, the conventional plate theory is not applicable. So, the bending behavior is decoupled from membrane behavior and modeled individually using specialized shell elements based on elastic[62][63][64], elastic with temperature-dependent[18][65], and viscoelastic approach [66]. In[66], finite strain viscoelastic approach was proposed involving the generalized Maxwell and Voigt-Kelvin model. Also, the results of the deformation test from [40] were utilized to address the effect of deformation rate in FE model. Moreover, it was claimed that this method is applicable for both unidirectional and

woven reinforcement. The results derived from material characterization can lead to a suitable constitutive model that can depict the deformation mechanism.

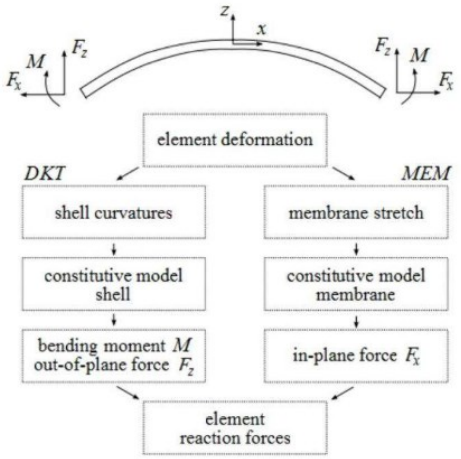

Figure 5. 2: decoupling flow chart [61]

In order to compare and validate the suitability of our material characterization obtained from the experiment, finite element analysis was conducted using ABAQUS standard software. In this section, the relaxation test and bending test are simulated and compared with test results. In addition, since viscoelastic materials are rate dependent, it was tried to simulate a test setup in the ABAQUS platform to demonstrate the effect of forming rate on uncured prepreg.

5.1 Relaxation test simulation

The geometry of the sample was modeled as a planar shell with a known dimension similar to the test sample. The element type was defined as CPS4R (4-node bilinear plane stress quadrilateral, reduced integration, hourglass control). The mesh control was set to structured with the size of 10mm. The material properties were defined same as the test sample, which is provided in table 4.4. Considering that the material is a viscoelastic material, two types of modulus were defined, instantaneous young modulus as well as relaxation modulus. To determine the relaxation modulus, time-domain was identified by proxy series. As already stated, the number of prony series is important in depicting the viscosity behavior. More terms would not necessarily result in a better answer, so the fitting goodness criteria should be considered when choosing the proper number of terms. Here four types of prony series in terms of the number of terms were fitted to the actual relaxation test fig. The corresponding prony coefficient through the optimization method that was already discussed and the goodness of the fit is characterized with MSE.table 5.1

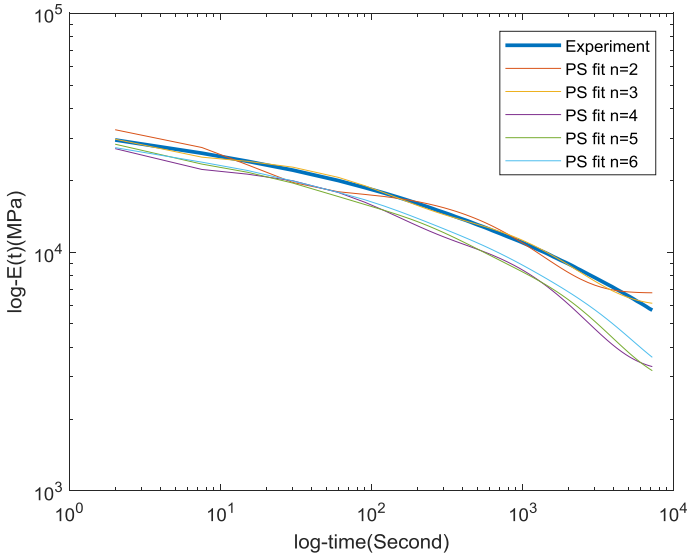

Figure 5. 3: The relaxation test in log-log scale fitted by four types of prony series model

For better illustration, Figure 5.4 shows the best model accompanied with the tests data individually.

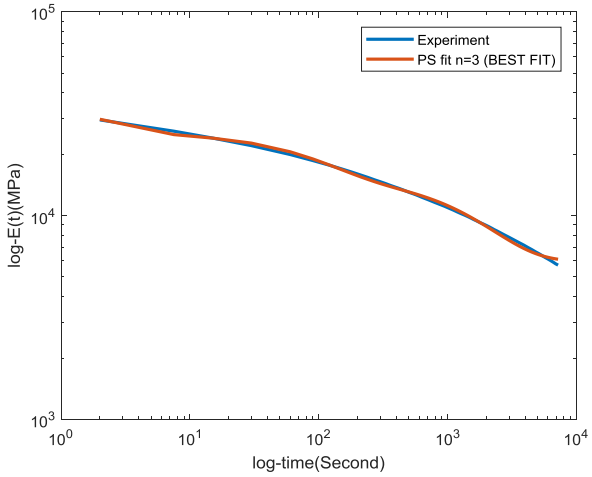

Figure 5. 4: Prony Best Model Fit

Number of Terms / Model Parameters	2	3	4	5	6
R_1	6747.57	5976.30	3187.83	2765.04	2740.19
R_2	11719.44	9473.23	9473.13	6901.77	5934.06
R_3	16559.79	12397.87	12398.00	7179.22	9275.15
R_4		10041.64	10041.63	10371.22	5482.61
R_5			3194.18	2748.94	2756.98
R_6				8060.70	7054.51
R_7					5341.93
η_1	∞	∞	∞	∞	∞
η_2	0.001038	0.000597	0.000597	0.035856	0.009868
η_3	0.080997	0.517121	0.517102	0.003997	0.858375
η_4		0.01022	0.01022	0.720745	0.070811
η_5			1.358161	0.311635	2.644907
η_6				0.000409	0.000288
η_7					0.001929
MSE ($\times 10^5$)	8.2	0.7	76.9	68.7	44.1

Table 5. 1: Prony Series parameters extracted from the fitting process

Based on the result available in table 5.1. The prony series composed of three exponential terms represents the best fitting because it has the lowest MSE value among other types. Hence, the prony coefficient corresponding to the best model could be a suitable selection for our study. The definition of prony to CAE software is different. Equation 4.11 indicated the general formation of prony series. In ABAQUS, the physical parameters are introduced dimensionless or regardless of their units. The constitutive parameters of prony series in ABAQUS are represented by g_i and τ_i

$$g_i = \frac{E_i}{E_0}, \qquad \tau_i = \frac{\eta_i}{R_i} \tag{5.1}$$

g_i is the normalized form of E, τ_i denotes the inverse of η / E, and E_0 is the instant modulus or relaxation modulus at t=0, which is also entered as an instantaneous module in the software. Table 5.2 shows the required input of values in ABAQUS. By defining these parameters, the viscoelastic feature of the material is completely defined.

The simulation was divided into two loading steps. In the first step, the displacement is applied in 1s, and in the second step, the displacement remains constant for 7200s. The ABAQUS solver

which was selected for this analysis is VISCOS*. The sample was fixed at one end, and the boundary condition was determined as encastre where all displacements were kept zero (U1=U2=U3=UR1=UR2=UR3=0)

g_i	τ_i
0.250026	1675.042
0.327215	1.9337
0.26502756	97.847

Table 5. 2: Dimensionless Prony series coefficients input in ABAQUS

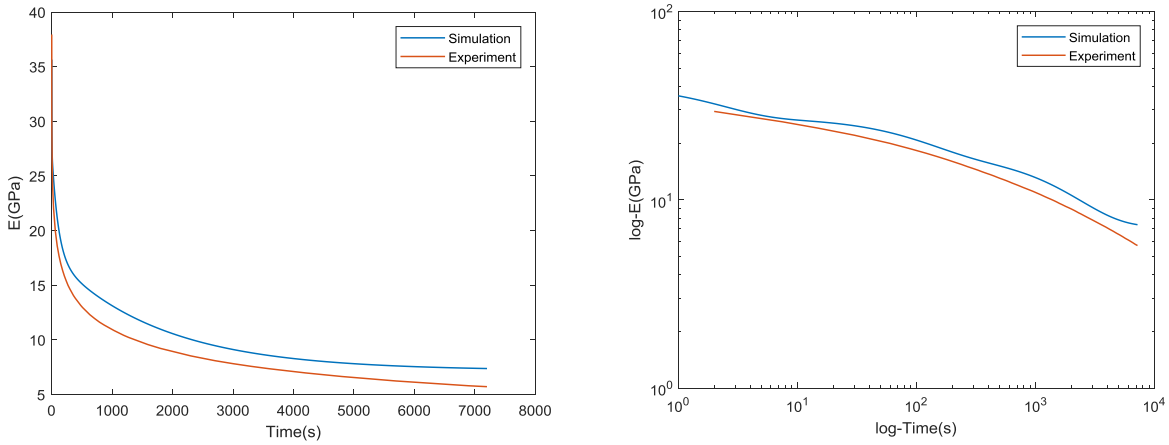

Figure 5. 5: Stress Relaxation experiment versus simulation results illustrated in linear and logarithmic scale

5.2 Bending Test Simulation

For this modeling, the sample was placed horizontally, and the geometry of the model was determined as 2D deformable beam. The element type was B21 (2-node linear beam in a plane) with 20 computational points. The material characteristics were defined similarly to the previous simulation. There are two steps of loading. In the first step, the beam was bent instantly under its own weight in STATIC* step. To represent the instant bending time the static during was set to 0.001s. The solver was selected as VISCOS* for the second step, and the step time was set corresponding to simulation duration. The boundary condition was chosen as encastre, and the loading was selected as body weight. The gravity constant was specified as 9.81m/s.

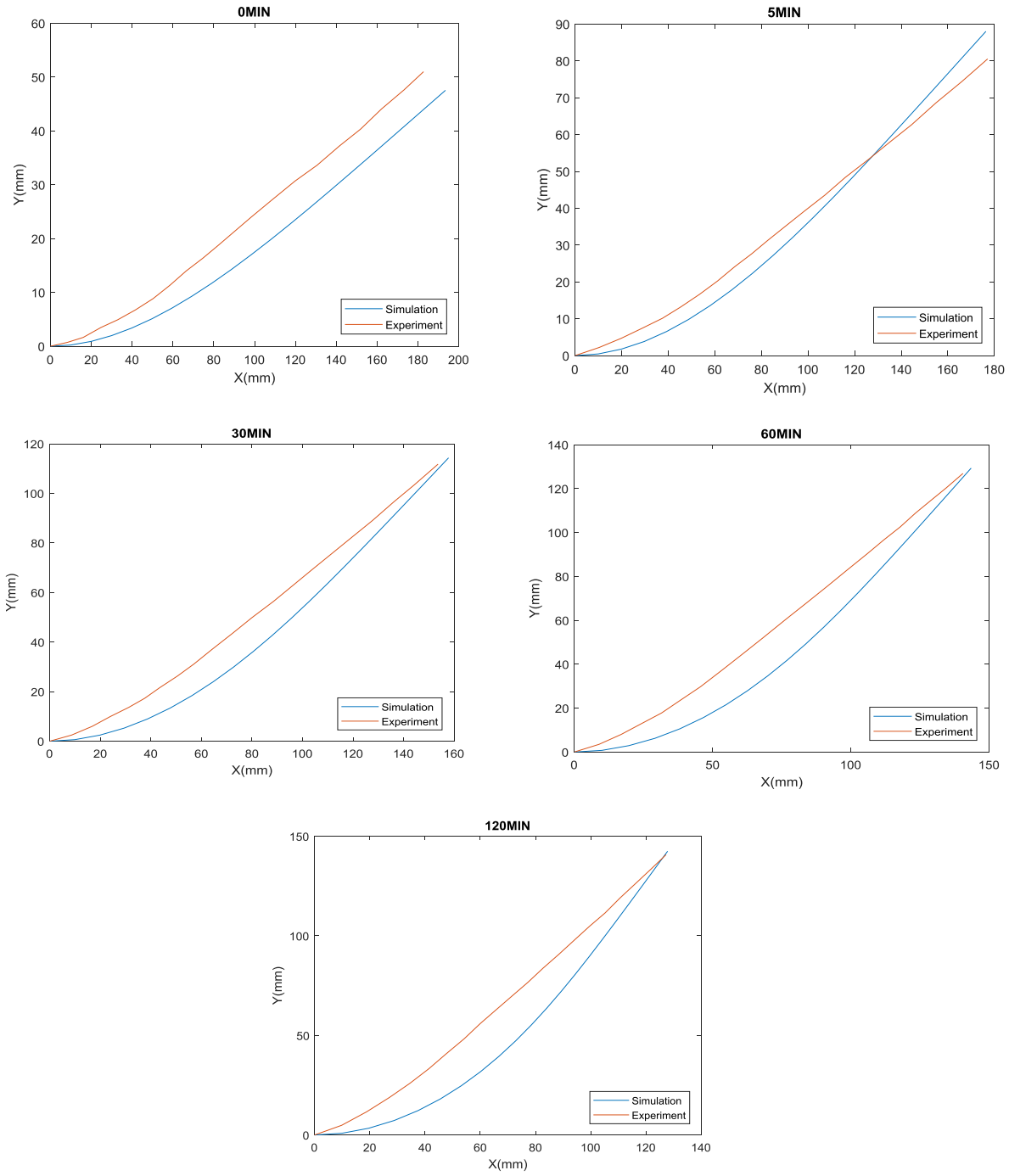

Figure 5. 6: X, Y coordinates of the bent sample derived from experiment and simulation in different time frame

5.3 Forming rate simulation

For the last section of finite element analysis, it was decided to depict the effect of bending rate on uncured prepreg. [67] Developed a test setup to observe the effect of deformation rate on textile prepreg. They placed the sample vertically, and a linear actuator applied the load at the end tip.

The applied moment versus deformed curvature is illustrated in Figure 5.8. The test was implemented for weft and wrap direction. The advantage of placing the sample vertically is that it can avoid any probable undesired twist in the sample during the loading. On the other hand, applying linear load may be problematic because it cannot produce pure bending in the sample, and slippage in the area of contact would happen. [40] Designed a new setup to provide pure bending on thermoplastic unidirectional composite. They attempted to eliminate any other deformation mechanism to represent a better result. The effect of bending rate was illustrated in terms of rotation angle and applied moment as well as the number of laminate layers in Figure 5.7. In our study, it was decided to repeat and simulate their work in ABAQUS by taking into account the viscoelastic feature. In our analysis to better satisfy the loading condition, the load was applied in a circular path.

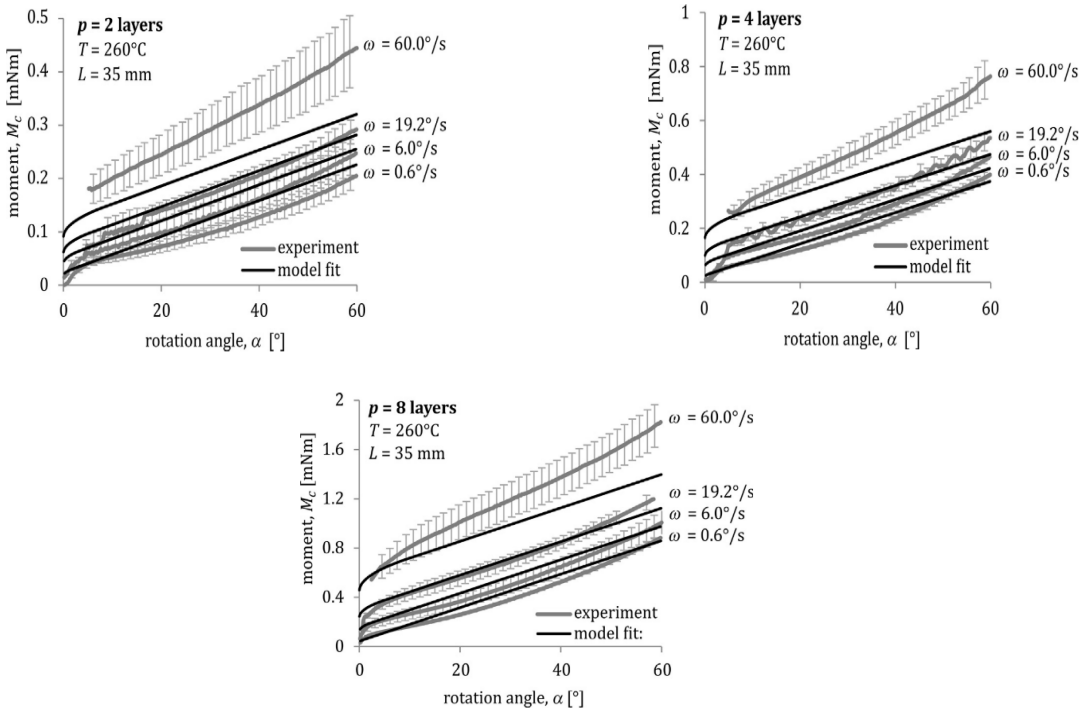

Figure 5. 7: Bending experiment with 2,4,8 layer composite implemented at 260 $^{\circ}C$ [40]

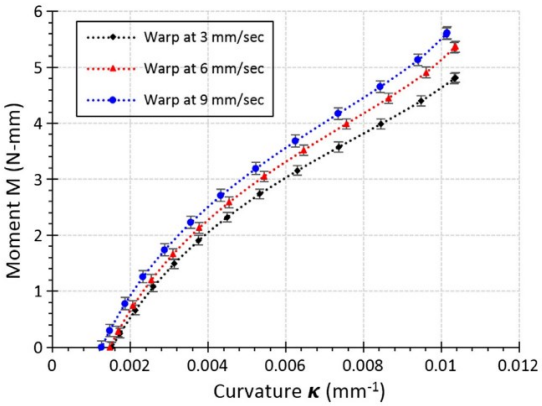

Figure 5. 8: The effect of bending rate represented in Bending moment versus curvature relation of 5HS prepreg in wrap direction [38]

In order to prepare the simulation in ABAQUS, similar to [38], the sample was placed vertically and fixed at one end. The beam was specified as a 2D wire beam with a length of 100mm. The material properties and element type was determined same as the preceding simulations. A circular 2D analytic rigid cell with a small radius was defined to represent the actuator tip in contact with the sample. The interaction between the actuator and the sample surface was determined as a normal hard contact, and tangential contact behavior was neglected. In order to provide a circular loading condition, first, the cell has to be tied to a reference point located at the middle of the beam. As the angular displacement is applied to the reference point, the rigid cell would rotate around the reference point as a center of rotation. Figure 5.9

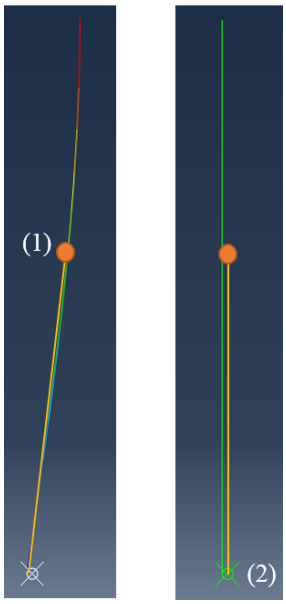

Figure 5. 9: the illustration of deformed and undeformed sample (1) reference point (center of rotation) (2) actuator tip

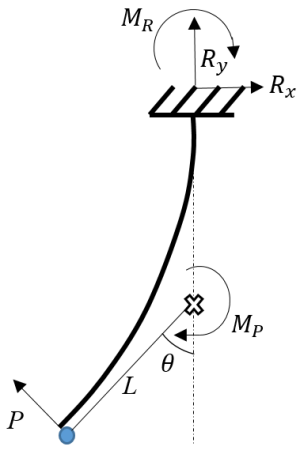

Figure 5. 10: Schematic drawing of system of samples and loading configuration

The applied load on the sample through the rigid cell (actuator) is always perpendicular to the surface Figure 5.10. By deriving the force equilibrium equations of the sample, it can be concluded that the applied load P is equal to the resultant force at the end fixed ($R = \sqrt{R_x^2 + R_y^2}$). The resultant reaction force can be derived through an ABAQUS solver. The relation between the resultant force and the applied moment from the actuator is M=PL, where L is the rotation radius.

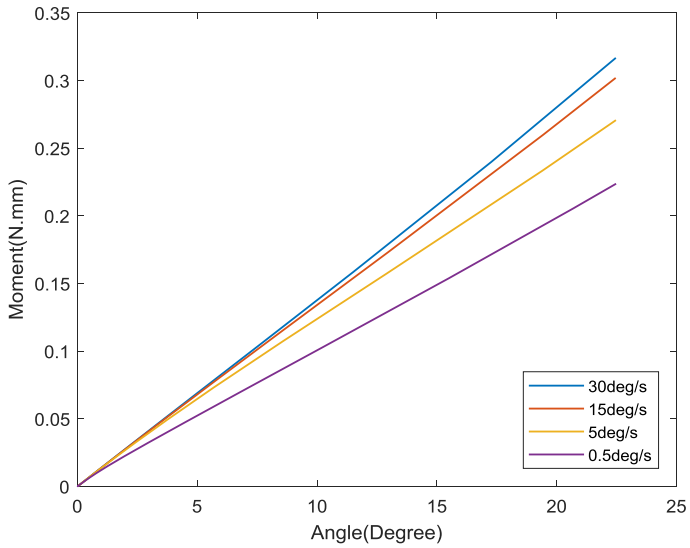

Figure 5. 11: The effect of bending rate in simulated deformation mechanism in ABAQUS

Figure 5.11 Depicted the amount of moment applied by the actuator as a function of deformation angle. It shows that the relation between these two parameters is linear, which is in good agreement with the results illustrated in [40]. The simulation was implemented for different deformation rates. Clearly, as the rate increases, the slope of the curve increases as well. It means, to deform the sample to a specific angle, a higher moment is required for a more loading rate. Besides, it can be

seen that the increase of slope is not continuing for higher rates; however, the value will converge to a certain threshold.

6 Conclusion

The goal of this study was focused on the investigation of the viscoelastic properties of unidirectional uncured prepreg and its contribution in depicting the bending deformation behavior at forming conditions. Different approaches in determining stress relaxation were proposed, and the difference between linear and nonlinear models was discussed. Then, the governing equations of bending behavior were derived with considering the viscoelastic feature.

The experiments carried out in this study were divided into four sections. First of all, After sample preparation, the relaxation test was implemented both in the room and at elevated temperature by using a tensile test machine instead of DMA because the sample is uncured and DMA cannot satisfy proper testing conditions. Then in order to observe the stress-strain relation of prepreg tensile test was conducted with the test setup same as relaxation test. Last but not least, the cantilever bending test was.

Various modeling approaches of viscoelastic behavior with different model parameters were discussed as well as our model. Also, the differences between linear and nonlinear models were addressed, and the best model was selected by comparing to the obtained experimental data. In addition, the reason for the deviation between the ideal and actual relaxation test was mentioned.

Two methods were introduced for governing the bending equations. The nonlinear partial integrodifferential equation for the linear model and integral approach for the nonlinear model. the results obtained from these approaches were verified by experimental observation. Also, the advantage and disadvantages of each method were indicated.

The effect of temperature was experimentally observed by following the time-temperature superposition principle the stress relaxation of the sample was studied for elevated temperatures. Experimental observation has shown that the horizontal shift factor (a_T) along with the fiber direction is not convinced by employing regular Arrhenius and Williams-Landel-Ferry(WLF) models. The investigation indicated that the relaxation master curve for nonlinear viscoelastic is not only a function of temperature but also the value of relaxation modulus.

In order to complement our study, the experimental observation and analytical resolution were evaluated by implementing finite element analysis at a macro scale in ABAQUS software. The relaxation testing condition and bending mechanism were simulated. The viscoelastic property obtained from the experiment was introduced to the software in PS formulation. Also, the effect

of the number of Prony terms was studied to Figure out the optimized number. Furthermore, a deformation action was modeled to depict the effect of the deformation rate.

6.1 Future work

Due to the advent of novel technologies in composite manufacturing, there are still significant challenges that provide precious opportunities for research. As an ending of this thesis, several recommendations for future work are presented as follows:

This study focused on the carbon fiber/epoxy prepreg UD composites, and it can be extended for other prepreg systems with different fiber and resin types and architecture. For instance, the effect of fiber volume fraction, yarn, or weave geometry can be presented.

Develop an experimental setup to eliminate or minimize the existing restrictions of test implementation. For example, come up with an idea to avoid the resin flow at elevated temperature and maximize the speed of instant elongation of the sample in relaxation test to approach ideal condition. Also, the interaction between tools and the sample can be considered to bring the experimental conditions as close as possible to the actual processing condition.

In this study, the stress relaxation and bending behavior of single-ply prepreg were investigated. It was recommended that the proposed approach be utilized for uncured laminate to observe the effect of inter-ply and intra-ply stress relaxation behavior to gain a better understanding of this phenomenon.

During the forming or curing process, the sample experiences heating preceding cooling. So the study of the stress relaxation behavior during cooldown is also essential.

The effect of shear and tensile coupling on bending properties should be addressed because these are the real deformation mechanisms that happen during the actual forming process.

This study has covered the macroscale properties; however, the forming simulation is a multi-scale problem, where macroscopic behavior is highly dependent on the interaction of composites component at mesoscale and at the microscale. So the investigation of Mesoscale and microscale can be useful in better grasping the true behavior of the material. The interaction of fiber and matrix can be assumed as a fluid-structure interaction (FSI) which can be a powerful approach in demonstrating better numerical simulations.

Creep is known as another key feature in defining the viscoelastic behavior of the material, so the development of a constitutive model to describe the creep behavior is recommended.

It was mentioned earlier that the time-temperature superposition principle is limited to linear nonlinear. Therefore the closed-form formulation is required to extend this methodology for a broad range of materials

Based on the proposed methods for deriving bending equations, nonlinear partial integro-differential represents better results; however, it requires a creep compliance function. Equation 4.26 shows the relation between relaxation modulus and creep compliance. For the linear viscoelastic model, the conversion from stress modulus to creep compliance is feasible. But for the proposed nonlinear model, this is not possible. So achieving a closed-form solution for relaxation-creep conversion is recommended.

7 References

[1] L. Zhang, X. Wang, J. Pei, and Y. Zhou, "Review of automated fibre placement and its prospects for advanced composites," *J. Mater. Sci.*, vol. 55, doi: 10.1007/s10853-019-04090-7.

[2] "• Composites global market value 2027 | Statista." https://www.statista.com/statistics/944471/global-market-value-of-composites/ (accessed Jul. 29, 2021).

[3] A. Liberati *et al.*, "Manufacturing-Induced Imperfections in CompositeParts Manufactured via Automated Fiber Placement.pdf," *Nature*, vol. 388. pp. 539–547, 2018.

[4] S. Nagendra *et al.*, "N. Parthasarathy* *** Hewlett Packard Company Santa Rosa, California 95403 1.," *New York*.

[5] R. P. Smith, Z. Qureshi, R. J. Scaife, and H. M. El-Dessouky, "Limitations of processing carbon fibre reinforced plastic/polymer material using automated fibre placement technology," doi: 10.1177/0731684416659544.

[6] D. H. J. A. Lukaszewicz, C. Ward, and K. D. Potter, "The engineering aspects of automated prepreg layup: History, present and future," *Compos. Part B Eng.*, vol. 43, no. 3, pp. 997–1009, 2012, doi: 10.1016/j.compositesb.2011.12.003.

[7] A. Beakou, M. Cano, J. B. Le Cam, and V. Verney, "Modelling slit tape buckling during automated prepreg manufacturing: A local approach," *Compos. Struct.*, vol. 93, no. 10, pp. 2628–2635, 2011, doi: 10.1016/j.compstruct.2011.04.030.

[8] M. Y. Matveev, P. J. Schubel, A. C. Long, and I. A. Jones, "Understanding the buckling behaviour of steered tows in Automated Dry Fibre Placement (ADFP)," *Compos. Part A Appl. Sci. Manuf.*, vol. 90, pp. 451–456, 2016, doi: 10.1016/j.compositesa.2016.08.014.

[9] M. Belhaj and M. Hojjati, "Wrinkle formation during steering in automated fiber placement: Modeling and experimental verification," doi: 10.1177/0731684417752872.

[10] N. Bakhshi, "Process-Induced Defects during Tow Steering in Automated Fiber Placement: Experiment, Modeling and Simulation," no. November, pp. 1–26, 2018.

[11] J. Sun, Y. Gu, M. Li, X. Ma, and Z. Zhang, “Effect of forming temperature on the quality of hot diaphragm formed C-shaped thermosetting composite laminates,” *J. Reinf. Plast. Compos.*, vol. 31, no. 16, pp. 1074–1087, 2012, doi: 10.1177/0731684412453778.

[12] Y. R. Larberg and M. Åkermo, “On the interply friction of different generations of carbon/epoxy prepreg systems,” *Compos. Part A Appl. Sci. Manuf.*, vol. 42, no. 9, pp. 1067–1074, 2011, doi: 10.1016/j.compositesa.2011.04.010.

[13] J. Sun, M. Li, Y. Gu, D. Zhang, Y. Li, and Z. Zhang, “Interply friction of carbon fiber/epoxy prepreg stacks under different processing conditions,” *J. Compos. Mater.*, vol. 48, no. 5, pp. 515–526, 2014, doi: 10.1177/0021998313476320.

[14] B. Zhu, T. X. Yu, and X. M. Tao, “An experimental study of in-plane large shear deformation of woven fabric composite,” *Compos. Sci. Technol.*, vol. 67, no. 2, pp. 252–261, 2007, doi: 10.1016/j.compscitech.2006.08.011.

[15] G. Lebrun, M. N. Bureau, and J. Denault, “Evaluation of bias-extension and picture-frame test methods for the measurement of intraply shear properties of PP/glass commingled fabrics,” *Compos. Struct.*, vol. 61, no. 4, pp. 341–352, Sep. 2003, doi: 10.1016/S0263-8223(03)00057-6.

[16] P. Boisse, N. Hamila, E. Vidal-Sallé, and F. Dumont, “Simulation of wrinkling during textile composite reinforcement forming. Influence of tensile, in-plane shear and bending stiffnesses,” *Compos. Sci. Technol.*, vol. 71, no. 5, pp. 683–692, 2011, doi: 10.1016/j.compscitech.2011.01.011.

[17] P. Harrison, M. J. Clifford, and A. C. Long, “Shear characterisation of viscous woven textile composites: a comparison between picture frame and bias extension experiments,” *Compos. Sci. Technol.*, vol. 64, no. 10–11, pp. 1453–1465, Aug. 2004, doi: 10.1016/j.compscitech.2003.10.015.

[18] E. Guzman-Maldonado, N. Hamila, P. Boisse, and J. Bikard, “Thermomechanical analysis, modelling and simulation of the forming of pre-impregnated thermoplastics composites,” *Compos. Part A Appl. Sci. Manuf.*, vol. 78, pp. 211–222, 2015, doi: 10.1016/j.compositesa.2015.08.017.

[19] I. Taha, Y. Abdin, and S. Ebeid, “Comparison of picture frame and Bias-Extension tests for the characterization of shear behaviour in natural fibre woven fabrics,” *Fibers Polym.*,

vol. 14, no. 2, pp. 338–344, 2013, doi: 10.1007/s12221-013-0338-6.

[20] R. P. Mohan, H. Alshahrani, and M. Hojjati, "Investigation of intra-ply shear behavior of out-of-autoclave carbon/epoxy prepreg," *J. Compos. Mater.*, vol. 50, no. 30, pp. 4251–4268, Dec. 2016, doi: 10.1177/0021998316635238.

[21] K. Potter, C. Langer, B. Hodgkiss, and S. Lamb, "Sources of variability in uncured aerospace grade unidirectional carbon fibre epoxy preimpregnate," *Compos. Part A Appl. Sci. Manuf.*, vol. 38, no. 3, pp. 905–916, 2007, doi: 10.1016/j.compositesa.2006.07.010.

[22] L. M. Dangora, C. Mitchell, K. D. White, J. A. Sherwood, and J. C. Parker, "Characterization of temperature-dependent tensile and flexural rigidities of a cross-ply thermoplastic lamina with implementation into a forming model," *International Journal of Material Forming*, vol. 11, no. 1. pp. 43–52, 2018, doi: 10.1007/s12289-016-1327-2.

[23] W. Zhang *et al.*, "Experimental methods to characterize the woven composite prepreg behavior during the preforming process," *Proc. Am. Soc. Compos. - 31st Tech. Conf. ASC 2016*, pp. 1–12, 2016.

[24] F. T. Peirce, "26—The 'handle' of cloth as a measurable quantity," *J. Text. Inst. Trans.*, vol. 21, no. 9, pp. T377–T416, Jan. 1930, doi: 10.1080/19447023008661529.

[25] C. Test, H. L. Test, T. Textiles, F. Test, and F. Test, "Standard Test Method for Stiffness of Fabrics 1," pp. 1–6, 2015, doi: 10.1520/D1388-18.2.

[26] P. Y. T. Henry, "Bending properties of a macroalga: Adaptation of Peirce's cantilever test for in situ measurements of Laminaria digitata (Laminariaceae)," *Am. J. Bot.*, vol. 101, no. 6, pp. 1050–1055, 2014, doi: 10.3732/ajb.1400163.

[27] M. Wei, "The theory of the cantilever stiffness test," *J. Text. Inst.*, vol. 80, no. 1, pp. 98–106, 1989, doi: 10.1080/00405008908659188.

[28] E. de Bilbao, D. Soulat, G. Hivet, and A. Gasser, "Experimental Study of Bending Behaviour of Reinforcements," *Exp. Mech.*, vol. 50, no. 3, pp. 333–351, 2010, doi: 10.1007/s11340-009-9234-9.

[29] B. Liang, N. Hamila, M. Peillon, and P. Boisse, "Analysis of thermoplastic prepreg bending stiffness during manufacturing and of its influence on wrinkling simulations," *Compos. Part A Appl. Sci. Manuf.*, vol. 67, pp. 111–122, 2014, doi:

10.1016/j.compositesa.2014.08.020.

[30] D. Soteropoulos, K. Fetfatsidis, J. A. Sherwood, and J. Langworthy, “Digital method of analyzing the bending stiffness of non-crimp fabrics,” *AIP Conf. Proc.*, vol. 1353, no. 2011, pp. 913–917, 2011, doi: 10.1063/1.3589632.

[31] L. M. Dangora, C. Mitchell, K. D. White, J. A. Sherwood, and J. C. Parker, “Characterization of temperature-dependent tensile and flexural rigidities of a cross-ply thermoplastic lamina with implementation into a forming model,” *Int. J. Mater. Form.*, vol. 11, no. 1, pp. 43–52, 2018, doi: 10.1007/s12289-016-1327-2.

[32] S. V. Lomov, I. Verpoest, M. Barburski, and J. Laperre, “Carbon composites based on multiaxial multiply stitched preforms. Part 2. KES-F characterisation of the deformability of the preforms at low loads,” *Compos. Part A Appl. Sci. Manuf.*, vol. 34, no. 4, pp. 359–370, Apr. 2003, doi: 10.1016/S1359-835X(03)00025-3.

[33] S. Kawabata, M. Niwa, and H. Kawai, “3—The finite-deformation theory of plain-weave fabrics part I: The biaxial-deformation theory,” *J. Text. Inst.*, vol. 64, no. 1, pp. 21–46, 1973, doi: 10.1080/00405007308630416.

[34] T. A. Martin, D. Bhattacharyya, and I. F. Collins, “Bending of fibre-reinforced thermoplastic sheets,” *Compos. Manuf.*, vol. 6, no. 3–4, pp. 177–187, 1995, doi: 10.1016/0956-7143(95)95009-N.

[35] J. Wang, A. C. Long, and M. J. Clifford, “Experimental measurement and predictive modelling of bending behaviour for viscous unidirectional composite materials,” *Int. J. Mater. Form.*, vol. 3, no. SUPPL. 2, pp. 1253–1266, 2010, doi: 10.1007/s12289-009-0670-y.

[36] A. Margossian, S. Bel, and R. Hinterhoelzl, “Bending characterisation of a molten unidirectional carbon fibre reinforced thermoplastic composite using a Dynamic Mechanical Analysis system,” *Compos. Part A Appl. Sci. Manuf.*, vol. 77, pp. 154–163, 2015, doi: 10.1016/j.compositesa.2015.06.015.

[37] S. Ropers, M. Kardos, and T. A. Osswald, “A thermo-viscoelastic approach for the characterization and modeling of the bending behavior of thermoplastic composites,” *Compos. Part A Appl. Sci. Manuf.*, vol. 90, pp. 22–32, Nov. 2016, doi: 10.1016/j.compositesa.2016.06.016.

[38] H. Alshahrani and M. Hojjati, “A new test method for the characterization of the bending behavior of textile prepregs,” *Compos. Part A Appl. Sci. Manuf.*, vol. 97, pp. 128–140, 2017, doi: 10.1016/j.compositesa.2017.02.027.

[39] R. Sourkia, S. S. N. , B. Khatira, b, and 1 , R. Vaziria, 1, A.S. Milania, “Pure Bending Characterization of Dry Woven Textile Composites under Loading-Unloading Regimes: An Experimental Approach.”

[40] U. Sachs and R. Akkerman, “Viscoelastic bending model for continuous fiber-reinforced thermoplastic composites in melt,” *Compos. Part A Appl. Sci. Manuf.*, vol. 100, pp. 333–341, Sep. 2017, doi: 10.1016/j.compositesa.2017.05.032.

[41] G. Akovali, *Handbook of composite fabrication*. 2001.

[42] P. Roozbehjavan *et al.*, “Experimental and numerical study of distortion in flat, L-shaped, and U-shaped carbon fiber-epoxy composite parts,” *Journal of Applied Polymer Science*, vol. 131, no. 13. 2014, doi: 10.1002/app.40439.

[43] G. Twigg, A. Poursartip, and G. Fernlund, “Tool-part interaction in composites processing. Part I: Experimental investigation and analytical model,” *Compos. Part A Appl. Sci. Manuf.*, vol. 35, no. 1, pp. 121–133, 2004, doi: 10.1016/S1359-835X(03)00131-3.

[44] W. Lafayette, “Composite during loading and unloading,” *J. Compos. Mater.*, vol. 36, no. 06, pp. 745–755, 2002, doi: 10.1106/002199802023477.

[45] P. Shrotriya and N. R. Sottos, “Creep and relaxation behavior of woven glass/epoxy substrates for multilayer circuit board applications,” *Polymer Composites*, vol. 19, no. 5. pp. 567–578, 1998, doi: 10.1002/pc.10130.

[46] Solvay, “Technical Data Sheet CYCOM ® 977-2 and 977-2A PREPREG,” 2020.

[47] M. Nakada, “Accelerated testing methodology for long-term creep and fatigue strengths of polymer composites,” *Creep Fatigue Polym. Matrix Compos.*, pp. 325–348, Jan. 2019, doi: 10.1016/B978-0-08-102601-4.00011-4.

[48] M. Carboni, “Elastic Tensile Properties of Uncured Towpreg Composite Materials : Experiment and Modelling Concordia University,” no. August, 2020.

[49] Frank van Steenbergen and A. Tuinhof, *Nonlinear Approaches in Engineering Applications*. 2009.

[50] T. T. B. Laboratories and M. Hi, “Power-law behavior in the viscosity of supercooled liquids,” vol. 34, no. 3, pp. 1835–1840, 1986.

[51] M. L. Williams, R. F. Landel, and J. D. Ferry, “The Temperature Dependence of Relaxation Mechanisms in Amorphous Polymers and Other Glass-forming Liquids,” *J. Am. Chem. Soc.*, vol. 77, no. 14, pp. 3701–3707, 1955, doi: 10.1021/ja01619a008.

[52] K. J. Laidler, “The development of the arrhenius equation,” *J. Chem. Educ.*, vol. 61, no. 6, pp. 494–498, 1984, doi: 10.1021/ed061p494.

[53] M. Belhaj and M. Hojjati, “Wrinkle formation during steering in automated fiber placement: Modeling and experimental verification,” *J. Reinf. Plast. Compos.*, vol. 37, no. 6, pp. 396–409, 2018, doi: 10.1177/0731684417752872.

[54] Q. Xu, B. Engquist, M. Solaimanian, and K. Yan, “A new nonlinear viscoelastic model and mathematical solution of solids for improving prediction accuracy,” *Sci. Rep.*, vol. 10, no. 1, Dec. 2020, doi: 10.1038/s41598-020-58240-y.

[55] “Numerical Optimization,” 2006, doi: 10.1007/978-0-387-40065-5.

[56] “Mean Squared Error (MSE).” https://www.probabilitycourse.com/chapter9/9_1_5_mean_squared_error_MSE.php (accessed Sep. 15, 2021).

[57] M. T. Grießer and P. M. Taylor, “The bending behaviour of fabrics: An energy approach,” *Math. Comput. Simul.*, vol. 41, no. 5–6, pp. 579–586, 1996, doi: 10.1016/0378-4754(95)00102-6.

[58] T. J. Lahey and G. R. Heppler, “Mechanical modeling of fabrics in bending,” *J. Appl. Mech. Trans. ASME*, vol. 71, no. 1, pp. 32–40, 2004, doi: 10.1115/1.1629757.

[59] M. L. Realf-F-", M. C. Boyce, and S. Backer, “A Micromechanical Model of the Tensile Behavior of Woven Fabric.”

[60] “Composites Simulation Software.” https://www.esi-group.com/products/composites (accessed Aug. 14, 2021).

[61] “Composite forming simulations | AniForm.” https://aniform.com/ (accessed Aug. 14, 2021).

[62] D. Soulat, A. Cheruet, and P. Boisse, “Simulation of continuous fibre reinforced thermoplastic forming using a shell finite element with transverse stress,” *Comput. Struct.*, vol. 84, no. 13–14, pp. 888–903, 2006, doi: 10.1016/j.compstruc.2006.02.011.

[63] S. Allaoui *et al.*, “Experimental and numerical analyses of textile reinforcement forming of a tetrahedral shape,” *Compos. Part A Appl. Sci. Manuf.*, vol. 42, no. 6, pp. 612–622, 2011, doi: 10.1016/j.compositesa.2011.02.001.

[64] S. P. Haanappel, R. H. W. Ten Thije, U. Sachs, B. Rietman, and R. Akkerman, “Formability analyses of uni-directional and textile reinforced thermoplastics,” *Compos. Part A Appl. Sci. Manuf.*, vol. 56, pp. 80–92, 2014, doi: 10.1016/j.compositesa.2013.09.009.

[65] E. Guzman-Maldonado, N. Hamila, N. Naouar, G. Moulin, and P. Boisse, “Simulation of thermoplastic prepreg thermoforming based on a visco-hyperelastic model and a thermal homogenization,” *Mater. Des.*, vol. 93, pp. 431–442, 2016, doi: 10.1016/j.matdes.2015.12.166.

[66] D. Dörr, F. J. Schirmaier, F. Henning, and L. Kärger, “A viscoelastic approach for modeling bending behavior in finite element forming simulation of continuously fiber reinforced composites,” *Compos. Part A Appl. Sci. Manuf.*, vol. 94, pp. 113–123, 2017, doi: 10.1016/j.compositesa.2016.11.027.

[67] H. Alshahrani and M. Hojjati, “A new test method for the characterization of the bending behavior of textile prepregs,” *Compos. Part A Appl. Sci. Manuf.*, vol. 97, pp. 128–140, Jun. 2017, doi: 10.1016/j.compositesa.2017.02.027.